



Quantification of the near-surface wind conditions of the African coast: A comparative approach (satellite, NCEP CFSR and WRF-based)

Z.O. Olaofe ^{a, b,*}

^a Climate and System Analysis Group, University of Cape Town, Rondebosch, South Africa

^b ZakkWealth Energy, NG, Nigeria



ARTICLE INFO

Article history:

Received 1 June 2019

Received in revised form

28 August 2019

Accepted 26 September 2019

Available online 1 October 2019

Keywords:

Offshore wind power

WRF-Simulation

Sea surface temperature

Remote sensing

NCEP CFSR

Africa

ABSTRACT

The temporal and spatial variations of the near-surface wind conditions across the African coast are enormous due to local flow perturbations from changes in sea surface roughness or/and the weather system processes driven mainly by the Atlantic and Indian Ocean Currents. Over the past decades, the patterns of the near surface wind speed and directional flow have significantly changed across the globe. To quantify the long-term changes of the surface wind conditions off the African coasts, the spatial distributions of historical wind climates and analyzed surface temperature from remote sensing and two atmospheric models are presented. Thus, the offshore wind conditions variability derived across 4 coastal zones are quantified through a comparative approach. Over period of 2001–2010, the trends of regional-scale wind conditions from the numerical model of NCEP CFSR and satellite observations of CCMP are assessed. For identification of geographical viable locations with concentrated energy resource and negative temperature gradient, the surface wind conditions are adjusted to offshore turbine generator (V80 2 MW) operating height of 100 m. Based on statistical evaluation of the offshore wind condition, graphical representations of the historical wind climate are presented. Furthermore, the monthly and seasonal sectorwise winds at 10 and 100 m ASL for 2002 are compared in determining how local perturbations had caused a drift in offshore wind flows within the boundary height of 100 m. On local-scale evaluation, the near-surface wind conditions derived from WRF are validated with NCEP and CCMP datasets. The long-term historical wind conditions in time and space revealed that the satellite, WRF and NCEP models are reliable tools in replication of the coastal wind conditions across the coasts of Africa. Results also indicate the southeast coast to be an energetic region with concentrated mean wind energy flux between 300 and 1580 W/m² (8.10–13.70 m/s), but subjects to coastal variations of strong weather processes. No persistent wind pattern was found when considering the variability of near-surface wind conditions from a low to high latitude.

© 2019 Elsevier Ltd. All rights reserved.

1. Introduction

Among the developed nations, the continuous growth in the wind energy industry as a result of wind farms increment and the application of offshore energy resource as one of the most cost-effective renewables have been attributed to: bulk electricity generation and availability; electric power grid expansion, accessibility and management; competitiveness in terms of power generation capacity of the turbine technology at operational full capacity, among others [1–3]. To determine the socio-economic benefits of

coastal energy resource at a potential turbine site, an understanding of the changes in the atmospheric conditions and its impact on the distribution of offshore wind speed and sectorwise wind flow is essential [4].

For understanding of the synoptic processes of the offshore and its impacts on the boundary layer wind profile, a number of literature [5–9] had considered the importance of studying the long-term wind speed patterns and the effects of local perturbations on near surface wind profile within the atmospheric layer of 1000 m height [10–13]. From studied findings, results had shown that the information on temporal and spatial variations of the surface wind profile within the height of 200 m AGL/ASL are vital in: ¹accurate assessment of the distribution of wind energy resource [14–16], ²logistics and planning of wind farms operation

* Climate and System Analysis Group, University of Cape Town, Rondebosch, South Africa.

E-mail address: zakky201@gmail.com.

Nomenclature		
RE	Renewable Energy	u_{wnd} u-component/zonal wind (m/s)
kW	KiloWatt	v_{wnd} v-component/meridional wind (m/s)
MW	MegaWatt	v_{\min} Minimum Wind Speed
ws	Wind Speed (m/s)	v_{\max} Maximum Wind speed
wd	Wind Direction ($^{\circ}$)	WTG Wind Turbine Generator
ASL	Above Sea Level	n_x and n_y Grid points in the longitudinal and latitudinal directions, respectively
AGL	Above Ground Level	D Diameter (m) of swept area blades, A , (m^2)
RSS	Remote Sensing System	Z_o Standard surface roughness length (m)
SST	Sea Surface Temperature	v_{in}, v_{rated} and v_{out} cut-in, rated and cut-out wind speeds, respectively
WRF	Weather Research Forecasting	C_p Estimated capacity factor of WTG
WPD	Wind Power Density (W/m^2)	N, E, S, W and SW Northerly, Easterly, Southerly, Westerly and South-Westerly
GIS	Geographic Information System	ENE, ESE and NNW East-north easterly, East-south easterly and North-north westerly
GFS	Global Forecast System	SSE, WNW, WSW, NNE South-south easterly, West-north westerly, West-south westerly and North-north easterly
CSFR	Climate System Forecast Reanalysis	E, RPE, RAE Estimated error, relative percentage and absolute errors, respectively
NCEP	National Centers for Environmental Prediction	
CCMP	Cross Calibrated Multi-Platform	
ECMWF	European Centre for Medium-Range Weather Forecast	
MERRA	Modern Era-Retrospective Analysis for Research and Applications	

[17],³ understanding of the drifts in the wind speed and direction flow over a given time [18,19], though, primarily driven by weather system processes or/and local features of the surface [20].

On the regional-scale simulation and analysis of coastal wind conditions, the numerical weather prediction or Weather Research and Forecasting model (WRF), the satellite winds from RSS and the synoptic wind records/*in situ* dataset from reference stations (ships, meteorological towers, buoys and aircrafts) have been utilized [21–31] for assessing the temporal/spatial variations of the offshore energy resource through the physical and dynamic processes that operate below and above the atmospheric boundary layer.

To mention but few offshore energy studies conducted around the globe, the spatial variations of the coastal wind resource have been assessed with the statistical or/and dynamic downscaling methods. In assessing the suitability of the regional-scale wind conditions over the coast of China/China Seas Water, Liu et al. [32] utilized the 30-year regional ECMWF wind field dataset to run WRF model for production of the wind climates. Their studied findings show abundant wind energy resource over the East and South Sea of China (SCS) with estimated maximum annual wind power density (WPD) of $800 \text{ W}/\text{m}^2$ at 90 m. Also, Chang et al. [33] assessed the offshore wind resource on the SCS with multiple satellite ocean winds (ASCAT and SAR) and WRF-simulations. To assess the reliability of the satellite-borne wind retrievals, these high-resolution datasets were validated with *In Situ* winds of 7 coastal masts before assimilated into the WRF model. Upon modeling, the spatial distribution of the offshore wind speed at 100 m was assessed and WPDs were estimated at 400–600 W/m^2 . In further study, the ability of HY-2A scatterometer and radiometric WindSat in reproducing the surface wind speed and direction was examined by Zheng et al. [34] and results show good correlation between these sensors with estimated mean bias and root mean square error of 0 and 1.13 m/s, respectively. Furthermore, the ability of the ASCAT in reproducing the near-surface winds on the costal water of China was evaluated through validation of scatterometer with *in situ* observed winds at 13 moored buoys. From studied findings by Xu et al. [35], results show good performance of the scatterometer for a period of July 2013–Dec 2015.

At the west coast of India, the offshore energy resource derived

from the Oceansat-2 scatterometer (OSCAT) with GIS based methodology was assessed by Gadad and Deka [36]. The Authors were able to assess the spatial distribution of the offshore wind speeds and WPDs at 10 and 90 m. Also, from their sea depth classification of the west coast, more energy output from REpower 5 MW turbine was assessed with floating foundation (100–1000 m) than the monopile technology (0–35 m). Over the East and South Seas of Korean Peninsula, the satellite wind speed and direction from QuikSCAT at 10 m (Jan 2000–Dec 2008) were used to assess the offshore energy resource. From the findings by Jang et al. [37], an existence of high energy resource was reported for both Seas but considering the sea depth limitation, the West and Southwest coasts were discovered to be the most favorable zones for offshore wind farm development. Over the territorial water of Iberian Peninsula and surrounding ocean, Santos et al. [26] projected the future offshore wind speed and WPDs for different time spans (2019–2045, 2046–2072 and 2073–2099) based on CORDEX regional climate models (RCMs). From studied findings, these models were able to reproduce the wind conditions at 216 offshore points with an estimated mean speed bias of 10% while the future wind speed and power tend to decrease over most of the areas except for: the Atlantic coast of Galicia, Ebro Valley, North Portugal and Cape Gata, with increased winds. In addition to Iberian Peninsula, Carvalho et al. [27] assessed the performance of the WRF model in simulations of the ocean wind conditions by forcing 6 different reanalyzes. Their findings show that the WRF model driven by ERA interim could provide the most accurate initial and boundary conditions (datasets) for forcing the surface wind simulations over the onshore and offshore while the reanalysis of NCEP R2 could provide the most accurate offshore wind energy estimates [38]. For improved wind resource assessment, the preliminary verification of the modelled offshore winds with buoy winds shows good correlation with the observations.

Along the Coastal Zone of Oman Maritime, Charabi et al. [15] assessed the offshore wind resource with 3-km WRF model for wind atlas development. Cunden et al. [39] utilized the model for high resolution wind mapping over the Mauritius Island. At the Persian Gulf, Gholamreza et al. [40] assessed the wind resource for offshore energy estimation for 25-year (1984–2008). Based on the

ECMWF data across 550 grid points, their studied findings reveals the middle and southern regions to be high potential wind fields for electricity generation. Over the Arabian Sea and Bay of Bengal, the monthly and annual wind resource with satellite sensed dataset were assessed by Kumar et al. [41]. On regional scale over the Karnataka State (west coast of India), Gadad and Deja [36] assessed the offshore wind resource with the OSCAT data, GIS-based methodology and the REpower 5 MW turbine model for 2-year (2011–2012). Result findings show that the considered region had a high energy potential for power development and energy balancing across the Karnataka State.

From the reported studied findings above [15,21–40], the Authors presented the satellite derived, mesoscale modelled and the synoptic winds from *In Situ* datasets to be reliable tools in assessing the regional and local wind conditions for energy application.

For this study, the availability and distribution of the wind energy resource on the African coast are examined. For indepth understanding of the changes that occurs with the coastal wind conditions and assessment of the spatial distributions of the energy resource over four coastal zones of Africa (G1–G4, Fig. 1a) at 100 m height, this study utilized a 10-year satellite observations and validated with NCEP CFSR derived winds in measuring the degree of correlation (consistency) and its energy resource applicability. To estimate the seasonal/annual variations as well as its potential over the African coast, the near-surface wind conditions (daily, inter-monthly and seasonal) at a 10 m are adjusted to offshore WTG model (V80 2 MW) operating height of 100 m ASL. Furthermore, at geographical points (P1–P3, Fig. 1b) of the coastal region, the offshore wind climates derived from WRF, NCEP and satellite observations/CCMP for Jan–Dec 2009 are also assessed and compared. As response to RE development goals/needs across the continent, our studied aims are: ¹to assess the long-term trends (sectorwise monthly, seasonal, annual and inter-annual) of the coastal wind conditions at 100 m and offshore energy resource suitability for planning; ²to determine (compare) the monthly and seasonality of the sectorwise wind conditions at the southwest coast for 2002 only. These are vital in determining: ¹how the offshore energy resource had drifted over time as a result of local perturbations on the wind flow within the lowest boundary layer height; ² if NCEP wind conditions may be utilized for offshore wind resource generalization at the African coasts where in-situ data are

irrecoverable. Since no installed/operational wind farms exist on the coasts of Africa, the electricity production of Vesta 2000 kW model at 100 m, uniformly distributed over 98,200 WTG grids is compared with previous work carried out with 3000-kW model at 160 m height. With this comparison, the coastal energy resource can be fully explored with the deployment of suitable wind turbine model for energy planning. Following this introduction, the rest of the paper is structured: the offshore wind field and grid data selection are briefly discussed in section 2; Section 3 outlined the statistical model utilized for quantification of the regional wind conditions and the modeling of site power curve for typical 2000 kW WTG model. Results/discussion of the studied findings in comparisons with previous studied findings are reported in Section 4 while concluding remarks are presented in section 5.

2. Offshore wind field and data

The grid boundaries for the considered offshore wind field are mapped and identified (G1–G4, Fig. 1a) while the statistics of reference grids (P1–P3) in Fig. 1b are summarized in Columns 1–4 of Table 1. The mapped wind grids field covers the land and ocean surfaces of the African continent with estimated coverage area at 11736 km². G1 is situated on the South Atlantic Ocean at –3648 m elevation, G2 on the North Atlantic at –4304 m while G4 is relatively close to the Indian Ocean at –3441 m elevation. The satellite winds of the CCMP L3.0 ($0.25 \times 0.25^\circ$) and NCEP Climate Forecast System Reanalysis ($0.312 \times 0.312^\circ$) across the regional wind field (G1–G4) at 6-hourly interval from January 2001–December 2010 are obtained. For 10-year period, the considered parameters include: (1) u-component and v-component wind speeds at height of 10 m (2) analyzed SST from RSS at spatial subsetting of latitudes at 45° – 40° and longitudes of -20° – 50° . On local-scale evaluation, the wind datasets at reference points (P1–P3, Fig. 1b) are also assessed from two regional models (NCEP and WRF) and satellite observations for Jan–Dec 2009.

3. Methodology

3.1. Analysis of the coastal wind profiles

The offshore wind profiles are calculated from the time series of the u-component wind (m/s) at 10 height ($u_{\text{wind}10}$) and the v-

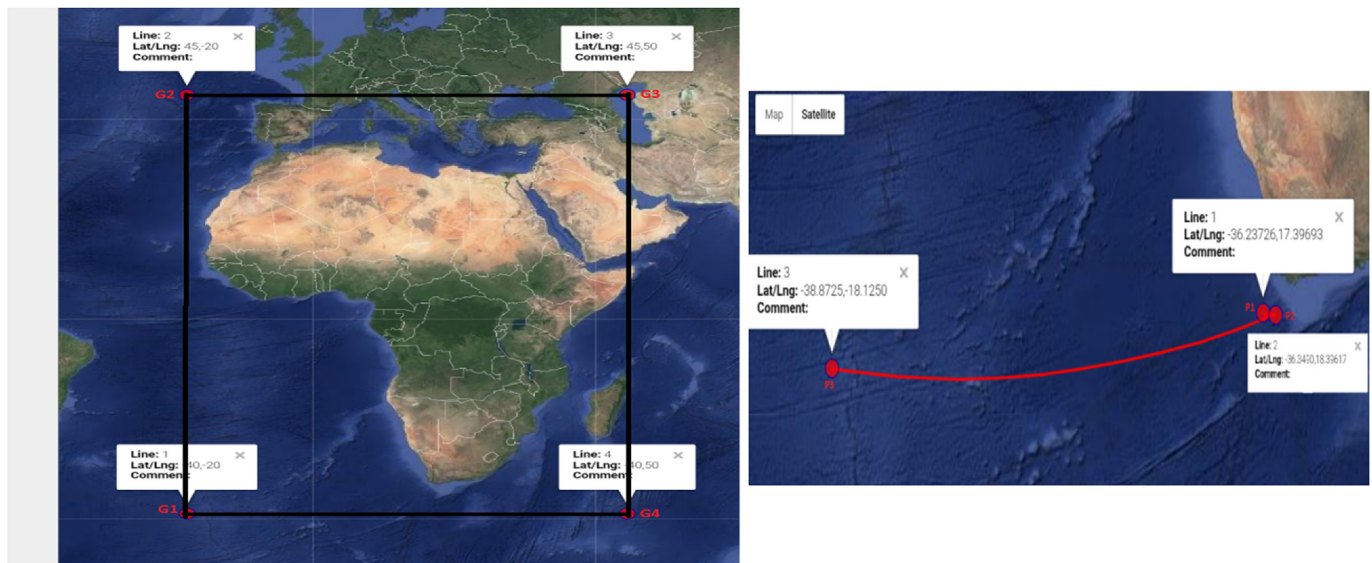


Fig. 1. Studied wind field (G1–G4) and geographical reference points (P1–P3) of the coastal region of Africa.

Table 1

Summary of site reference grid coordinates and wind power class at 10 m height ASL.

Reference (ID)	Longitude (E)	Latitude (N)	Depth (m)	Start date	End date	WPD (W/m ²)	Wind class
G1	-20.0000	-40.0000	-3648	01/01/2001	31/12/2010	532	7
G2	-20.0000	45.0000	-4304	01/01/2001	31/12/2010	379	6
G3	50.0000	45.0000	-25.6	01/01/2001	31/12/2010	128	2
G4	50.0000	-40.0000	-3441	01/01/2001	31/12/2010	465	7
P1	17.39693	-36.23726	-2689	01/01/2009	31/12/2009	330	6
P2	18.39617	-36.3490	-3830	01/01/2009	31/12/2009	349	6
P3	-18.1250	-38.8725	-3035	01/01/2009	31/12/2009	527	7

Wind classes: 1 = poor, 2 = Marginal, 3 = Fair, 4 = Good, 5 = Excellent, 6 = Outstanding, 7 = Superb [51].

component wind (m/s) at 10 m (v_{wind10}) as:

$$ws_{10} = \sqrt{(u_{wind10})^2 + (v_{wind10})^2} \quad (1)$$

where ws_{10} (m/s) is the time series of the calculated wind speed.

For the coastal wind flows, the mathematical equations are defined:

$$\text{for } u_{wind10} > 0 \text{ and } v_{wind10} > 0, wd_{10} = \left(270 - \left(\frac{180}{PI} * a \tan\left(\frac{v_{wind10}}{u_{wind10}}\right) \right) \right) \quad (2)$$

$$\text{for } u_{wind10} < 0 \text{ and } v_{wind10} < 0, wd_{10} = \left(90 - \left(\frac{180}{PI} * a \tan\left(\frac{v_{wind10}}{u_{wind10}}\right) \right) \right) \quad (3)$$

$$\text{for } u_{wind10} < 0 \text{ and } v_{wind10} > 0, wd_{10} = \left(90 - \left(\frac{180}{PI} * a \tan\left(\frac{v_{wind10}}{u_{wind10}}\right) \right) \right) \quad (4)$$

$$\text{for } u_{wind10} > 0 \text{ and } v_{wind10} < 0, wd_{10} = \left(270 - \left(\frac{180}{PI} * a \tan\left(\frac{v_{wind10}}{u_{wind10}}\right) \right) \right) \quad (5)$$

where wd_{10} (°) is the calculated wind direction at each grid point across the considered coastal wind field. For other wind conditions, they include: if ($u_{wind} = 0$) and ($v_{wind} > 0$), $wd_{10} = 180$; if ($u_{wind} < 0$) and ($v_{wind} = 0$), $wd_{10} = 90$; and if ($u_{wind} > 0$) and ($v_{wind} = 0$), $wd_{10} = 270$.

With Eqs (1)–(5), the time series of offshore wind speed and sectorwise direction at 100 m (ws_{100} and wd_{100} , respectively) are calculated from the adjusted zonal and meridional winds of 100 m height ($u_{wind100}$ and $v_{wind100}$) with reference to a 10 m winds in neutral atmospheric condition:

$$u_{wind100} = u_{wind10} \left[\frac{\ln\left(\frac{z_{100}}{z_o}\right)}{\ln\left(\frac{z_{10}}{z_o}\right)} \right] \quad (6)$$

$$v_{wind100} = v_{wind10} \left[\frac{\ln\left(\frac{z_{100}}{z_o}\right)}{\ln\left(\frac{z_{10}}{z_o}\right)} \right] \quad (7)$$

where $u_{wind100}$ and $v_{wind100}$ are the estimated zonal and meridional

winds (m/s), respectively, at 100 m; z_{100} and z_{10} are the proposed and reference heights of 100 and 10 m, respectively, while z_o is the coastal surface roughness = 0.0002 m (assuming uniformity).

¹Note: To correct for atmospheric effects on the coastal wind profiles in Eqs (6) – (7), time series of the Monin-Obukhov length (m) are required but unavailable for this study.

Next, the time series of the coastal wind speed ws_{100} and directional wd_{100} at 100 m are calculated from Eqs (1) – (5) above.

Furthermore, the geostrophic draw law (GDL) based on the friction velocity and coastal roughness at different grid points is considered for estimation of the geostrophic wind speed and direction with time. Thus, the cleansing procedure utilized by Larsen et al. [42] is considered with the estimated wind speed and direction (Eqs (1)–(7)) for refinement of the offshore wind speed and direction from local effects. Thus, the corrected wind speed and direction for the considered heights are obtained.

For a given surface roughness length and friction velocity of GDL, the corrected wind speed at 10 m height is calculated:

$$ws_{10}(z_{10}, z_o) = \frac{\hat{u}}{\kappa} \ln \frac{z_{10}}{z_o} \quad (8)$$

and the refined (standard) wind direction for the coast at 10 m height, z_{10} , is estimated:

$$wd_{10}(z_{10}, z_o) = \hat{\alpha}_G - \arcsin \frac{B\hat{u}}{\kappa\hat{G}} \quad (9)$$

where friction velocity is denoted as \hat{u} , $\kappa = 0.4$ is the von Kármán constant, the geostrophic wind speed as \hat{G} , and direction, $\hat{\alpha}_G$; B is the dimensionless parameter of GDL and dependent on the atmospheric stability. Assuming neutral stratification, the value of $B = -4.5$ for any coastal grid in the southern hemisphere.

²Note: Since very limited topographic datasets were available for this study, Eqs. (8)–(9) were tested with three offshore grid points in Fig. 1b.

For analysis of seasonal wind profiles, the time series of the estimated wind speed and direction are grouped into seasonal months of: Dec–Feb (DJF, summer), Mar–May (MAM, autumn), Jun–Aug (JJA, winter) and Sept–Nov (SON, spring).

The frequency distribution of the sectorwise wind speed at the considered heights are determined:

$$f(v, k, C) = \left(\frac{k}{C} \right) \left(\frac{v}{C} \right)^{k-1} \exp \left[- \left(\frac{v}{C} \right)^k \right] \quad (10)$$

where $f(v, k, C)$ is the probability of observing wind speed, $v = ws$ (m/s) for given time; k and C are the dimensionless shape and scale (m/s) parameters, respectively, of the Weibull distribution; $v > 0, k > 0, C > 0$.

Similarly, the cumulative probability function, $F(v, k, C)$, of the Weibull distribution is expressed as:

$$F(v, k, C) = 1 - \exp \left[- \left(\frac{v}{C} \right)^k \right] \quad (11)$$

The maximum likelihood estimator (MLE) for the dimensionless shape parameter k of the Weibull distribution function is expressed:

$$k = \left(\frac{\sum_{i=1}^N \ln(v_i) v_i^k}{\sum_{i=1}^N v_i^k} - \frac{\sum_{i=1}^N \ln(v_i)}{N} \right)^{-1} \quad (12)$$

Note: k value is obtained through iteration with an initial value of $k=2$ until convergence and N is the number of coastal wind speed samples at each grid.

The scale parameter C is estimated from the mean value of Weibull shape parameter using the MLE expressed:

$$C = \left(\frac{\sum_{i=1}^N v_i^k}{N} \right)^{\frac{1}{k}} \quad (13)$$

The offshore mean wind speed values (m/s) of the Weibull distribution is computed:

$$\bar{v} = CI \left(1 + \frac{1}{k} \right) \quad (14)$$

where Γ denotes the gamma function.

The offshore mean WPDs for each grid based on Weibull shape (dimensionless) and scale (m/s) parameters at 10 and 100 m heights ASL are estimated:

$$E(k, C) = \frac{P}{A} = \frac{1}{2} \rho C^3 I \left(1 + \frac{3}{k} \right) \oplus \quad (15)$$

where $E(k, C)$ are the estimated mean WPDs and air density (kg/m^3), respectively; A is the swept area (m^2) of the WTG model.

3.1.2. Turbine modeling of electric power generation

To assess the lowest (increasing) and highest wind power productions (decreasing thrust coefficient) for different wind conditions, a typical 2000 kW WTG (V80 2 MW) model at 100 hub is considered. The effects of the sectorwise wind flows on the turbine model in the range of 0.2 m/s are assessed by considering four classes of coastal wind speeds that pertain to WTG operations at 100 m height (Table 2):

- For $v_{in} < 4.0 \text{ m/s}$, the wind power output (P_o) = 0 kW for 2000 kW WTG model.
- Between $v_{in} \geq v < v_{rated}$; the P_o value ranges between 66.20 and 1995 kW
- Between $v_{rated} \geq v \leq v_{cut}$; the P_o value = 2000 kW.
- Above the cut-out wind speed of WTG, v (m/s) > v_{cut} ; the offshore wind power output P_o = 0 kW.

Table 2
Summary of the offshore wind turbine technical datasheet (V80-2000 kW).

Cut-in-wind speed (m/s)	Noominal wind speed (m/s)	Cut-out-wind speed (m/s)	Swept area of rotor blades, A (m^2)/Diameter (m)	Nomin power (kW)	Hub height (m)	Number of rotor blades	Generator type
4	15	25	5,027/80	2000	100	3	Asynchronous with OptiSpeed

Further to this, time series of the capacity factor of a typical WTG model are computed for different coastal wind conditions: $v_{in} < 4.0 \text{ m/s}$, $v_{in} \geq v < v_{rated}$, $v_{rated} \geq v \leq v_{cut}$ and v (m/s) > v_{cut} .

Based on the offshore wind speed variation (v , m/s) at each grid cell over a given time period T (hr), the electrical energy output, E_o , (kWh) of a typical WTG model is simulated [50]:

$$E_o(v) = \frac{1}{2} \rho A \int_0^T C_p(v) v^3 dt \quad (16)$$

where Eq. (16) denotes the electrical energy output of a typical WTG and C_p is the estimated capacity factor of WTG as a function of the offshore wind speed v (m/s).

The electrical energy generation (kWh) of a typical WTG based on the frequency distribution of the Weibull wind speeds over time period (T) at each grid point is computed:

$$E_o(v) = T \int_0^\infty P(v) f(v, k, C) du \quad (17)$$

Note: the electrical energy of a WTG for the wind variations at 0.2 m/s is simulated for frequency distribution of the offshore wind speeds at 10 and 100 m heights ASL.

3.1.3. Analysis of temporal and spatial variations of coastal wind

Because of the variance in the spatial grid spacing of the satellite ($0.25 \times 0.25^\circ$) and NCEP ($0.312 \times 0.312^\circ$), this pose a major setback in the validation of regional NCEP with satellite winds, leading to mismatch of each grid point across the entire wind field for the same temporal scale. For consideration of single grid, the NCEP could be validated with the satellite winds through a bilinear interpolation technique of the nearest four grid points within the considered field. Thus, for a given grid location (lon/lat) in Fig. 1b, the correlation or/and coastal wind profile for NCEP with satellite winds could be simply assessed by performing interpolation on the wind field. Alternatively, the spatial information of the offshore wind field could be determined by considering the annual bias of NCEP wind distribution for each grid point across the coast and compared with the spatial distributions of the satellite annual wind speed.

The correlation and discrepancy of the NCEP when compared with the satellite/CCMP are assessed based on the following:

$$ME = \frac{1}{N} \sum_{i=1}^N (ws_y - ws_x) \quad (18)$$

$$RPE(\%) = \frac{1}{N} \sum_{i=1}^N \frac{(ws_y - ws_x)}{ws_x} * 100 \quad (19)$$

$$RAE = \frac{1}{N} \sum_{i=1}^N \frac{|ws_y - ws_x|}{ws_x} \quad (20)$$

where ME (m/s), RPE and RAE denote the estimated mean, relative

percentage and absolute errors, respectively, of the coastal wind speeds; w_{sy} and w_{sx} are time series of the coastal wind speeds from the proceeding and current years, respectively, at a given time.

4. Results and discussion

4.1. Results

The studied findings for the entire coast of Africa (Fig. 1a) at 10 and 100 m hubs for the periods of 2001–2010 are reported in Fig. 2–28, S1 – S36 and Tables 1–7.

4.2. Discussion

4.2.1. Analyzed wind conditions—African coastal zones (2001–2010)

For optimal coastal turbine utilization and mitigation of the effects of offshore wind variations, the study of the seasonal and annual variability of the offshore wind speed and sectorwise wind flow as a function of the changes in atmospheric conditions is essential [25,43,44]. From east (E) to north (N) coast, the regional impacts of induced climate change were stronger and dominant off the west coast and E Coast, with significant changes in SST level. From the results (Figs a–b of 2–5) for the seasonal SSTs (January (summer), April (autumn), July (winter) and November (spring)), the slowdown of the coastal air motion at the Equator and Eastern Zone may have been influenced by differences in temperature gradients or coastal surface disturbance. Also, the drifts in the sectorwise wind flows may be attributed to finding reported by Liu et al. [16] and Yonglong et al. [45] (such as decrease in frequency of strong winds, moisture, coastal urbanization, human activities in the coastal zones or exploitation of marine resources, among others).

Off the S to W and E zones of Africa with a predominant high SST, a high spatial variation with slowdown of the offshore winds was recorded with enhance wind climates over a large area of the SE coast (Fig. 4c–d). Driven by changes in the weather processes of the Atlantic and India Oceans, an upward trend of increase SST was dominant off the west and E–Coast and downward trend along the SE-coast.

At 12:00 UTC (Figs a–b of 2–5), there was a significant change in ocean SST from mean value (290K) with estimated daily and monthly SST biases of $\pm 7\text{K}$. At the offshore, the W- and E–coasts had witnessed a significant rise in SST with a drift or slowdown in the offshore winds while the S–coast recorded a temperature declination. Thus, a spatial variation of the offshore energy flux does exist as a result of the motion of air molecules from one pressure region to another over the ocean surface (Figs. c–d of 2–5). Furthermore, the seasonal distributions of the regional SST were examined and characterized by two temperature gradients (Fig. 6). By comparing the analyzed SST of Jan 2001 with Jan 2002 (Fig a), Apr 2001 and Apr 2002 (Fig b), Jul 2001 and Jul 2002 (Fig c), and Nov 2001 with Nov 2002 (Fig d), evidences of SST anomalies from the eastern to some areas of the north coast were observed (Fig. 6) with intermonth drift of the sectorwise wind flows (Figs c–d of 2–5). Although, SST anomalies across the entire coast were obvious, the drifts in the dominant wind flow were seen from SW- and SE-coasts towards the NW coast. Thus, drifts in the offshore wind speed and direction, coastal upwelling intensity and cloudiness were good indications of the regional warming across African coast [46] while anomalies in the mean sea level pressure (MSLP) patterns and jet stream may have be responsible for spatial variations of the offshore winds along the coastal zones of Africa [47].

The distributions of annual wind speeds of the CCMP and NCEP

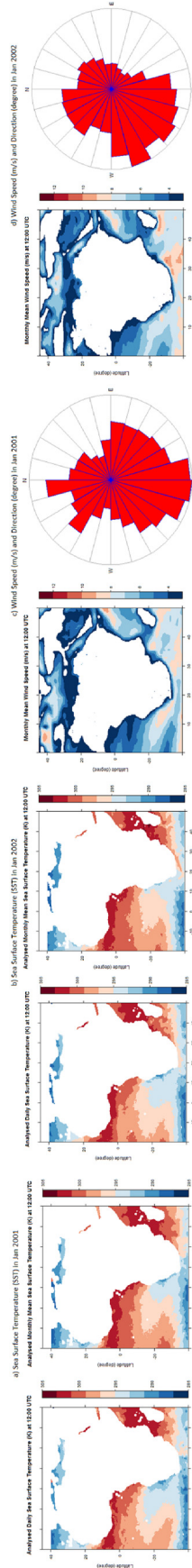


Fig. 2. Plot of the analyzed mean wind speed (m/s) and sectorwise wind direction ($^{\circ}$) as a function of sea surface temperature (K) derived from remote sensing for Jan 2001 and Jan 2002.

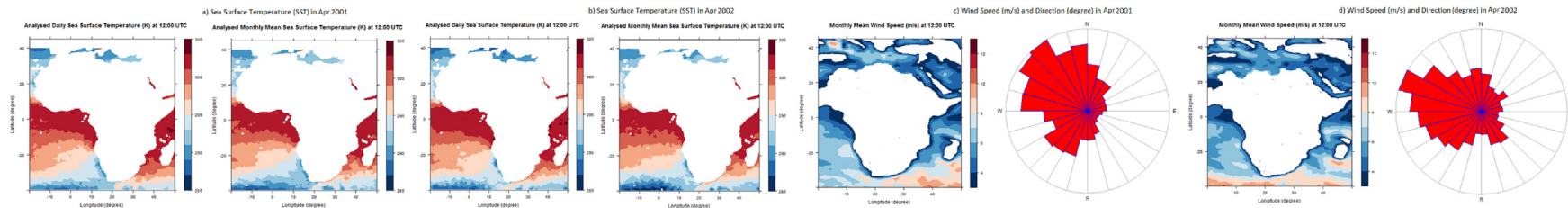


Fig. 3. Plot of the analyzed mean wind speed (m/s) and sectorwise wind direction ($^{\circ}$) as a function of sea surface temperature (K) derived from remote sensing for Apr 2001 and Apr 2002.

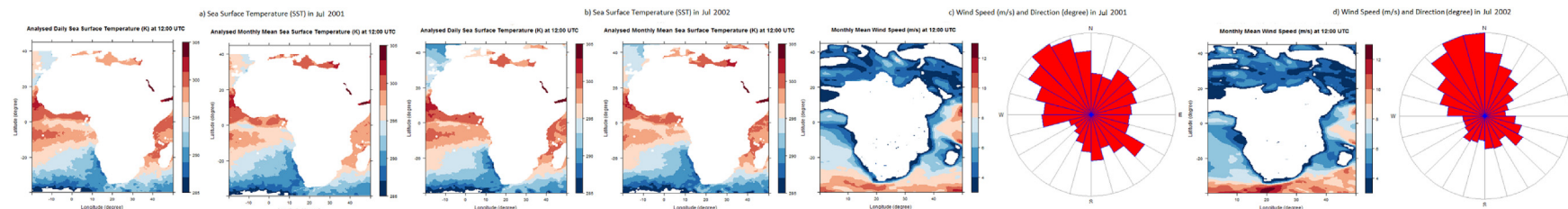


Fig. 4. Plot of the analyzed mean wind speed (m/s) and sectorwise wind direction ($^{\circ}$) as a function of sea surface temperature (K) derived from remote sensing for Jul 2001 and Jul 2002.

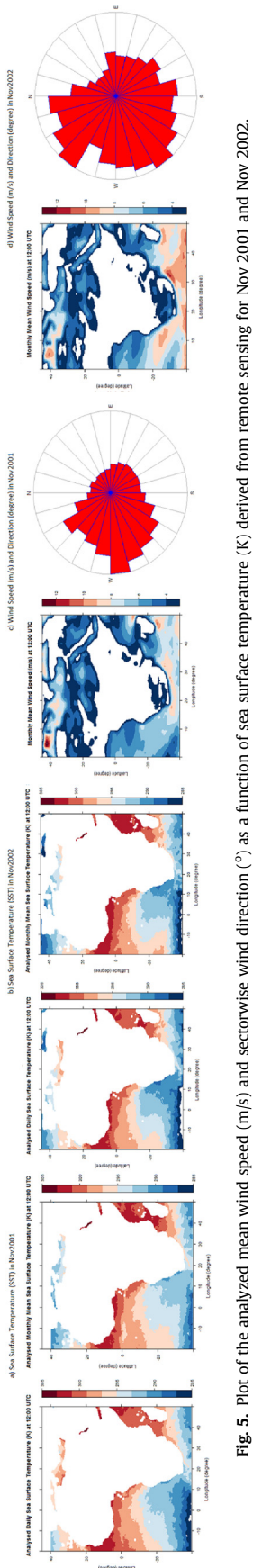


Fig. 5. Plot of the analyzed mean wind speed (m/s) and sectorwise wind direction (°) as a function of sea surface temperature (K) derived from remote sensing for Nov 2001 and Nov 2002.

at heights of 10 and 100 m from 2001 to 2010 have been analyzed (Figs. 7–10, S1–S6). Along the SE coast, some notable increase of the near-surface wind speed from 2001 to 2002, decrease in magnitude of the wind speed from 2002 to 2003, a significant increase from 2003 to 2005, changes in offshore wind patterns and significant slowdown of the wind distribution from 2005 to 2007 and 2008–2010 were recorded. Off the west coast, there were indications of high vulnerability of the coastal winds to regional climate changes mostly seen by SST increase and sea level rising. Across the entire coast, the inter-annual wind distributions (Figs a–b of 16–17) and the bi-annual wind variations (Table 3) were analyzed. The CCMP and NCEP were able to replicate the spatial variability of the offshore wind speed but with anomalies observation across large portion of the African coast from 2001 to 2010. At G1–G4 (Fig. 1a), the annual wind speeds (m/s) were analyzed and found to be non-monotonic at these grid cells. From 2001 to 2002, the increase trends of annual mean winds at G1, G2 and G4 were recorded, except at G3 (Table 4) while for the period of 2004–2005, increase of annual wind speed was recorded for the grids (G1–G4). Also, from 2008 to 2009, a slowdown of annual mean wind was seen at G1, G2 and G4, except at G3 with small increase in offshore wind speed (<0.5 m/s). Anomalies in the offshore wind speed at all grids were observed for the period of 10-year and attributed to the weather processes of the Atlantic and Indian oceans.

The monthly variations of the offshore wind speeds derived for 10-year of Jan 2001–Jan 2010 (Jan 2001, Jan 2002, ..., Jan 2009 and Jan 2010); February (Feb 2001–Feb 2010) to December of 2001–2010 (Dec 2001, Dec 2002, Dec 2009 and Dec 2010) have been analyzed (Fig. 11 and S7–S11). At 10 m, the inter-month wind distributions of the CCMP and NCEP were compared in determining: ¹the performance of the NCEP model and RSS in reproduction of the monthly winds and ²if changes in the monthly weather processes had resulted in drifts of the directional flow of the wind speed. Also, the comparisons of the inter-month wind speeds across G1–G4 were considered in assessing the spatial variance at different coastal grid zones as well as its energy potential. At G1 in South Atlantic coast (Fig. 1a), an estimated bi-annual bias (E , m/s) from CCMP shows an increase trend of the offshore winds from Jan–May of 2001–2002 with a downward trend in June (Fig a of S30–S31). For the period of 2002–2003, a decrease trend of the offshore wind from January–June was recorded with exception in February with a small increase in the magnitude of offshore wind speed. For the estimated NCEP biases at G1 (Fig b of S30–S31), an increase in inter-month wind speed was observed from Feb–Mar and May of 2001–2002 while the months of Jan, Apr and Jun recorded a slowdown of the offshore wind. Similarly, an increase in the offshore wind speed was also observed from 2002 to 2003 with exception (March, May–June) with a slowdown of coastal winds. Comparing the CCMP with NCEP inter-month wind speed, the estimated mean biases from 2001 to 2010 show that the NCEP (Fig b of S30–S32) failed to accurately reproduce the coastal wind speed at G1 (Fig a of S30–S32) especially for the periods of 2002–2004 and 2009–2010. As a result, Kulkarni et al. [48] in their findings emphasized the need to careful assess the performance of a RCM simulation before application to coastal wind. Meanwhile, at G1, the inter-month variations indicate an offshore wind anomaly in S coast where the energy resource peaks for the same period of years.

Due to dominant strong synoptic weather systems and their associated fronts [49], the most notable trends of offshore wind speeds occur at the SE and W regions with a slow drift of the near-surface wind conditions at the Equator (-18–20°N). In an offshore power conversion, the sectorwise wind flows become obvious [7] in analysis of the seasonal variations especially during the most

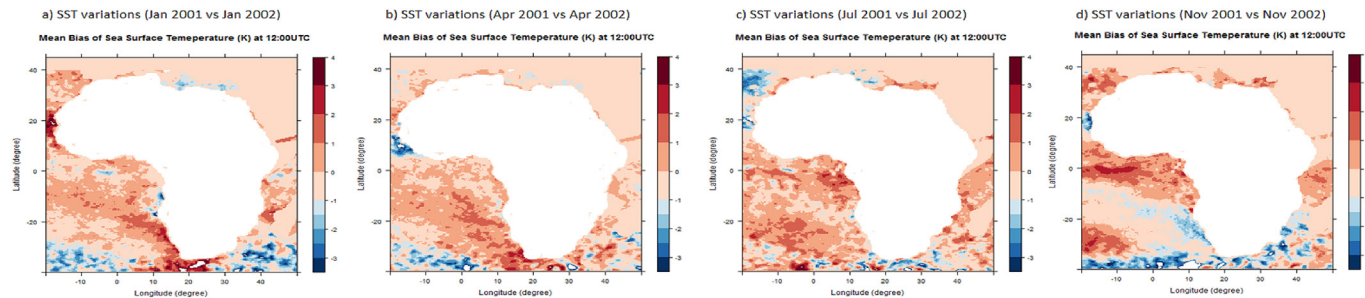


Fig. 6. Seasonal variation of regional sea surface temperature (SST, K) trend along the African coast.

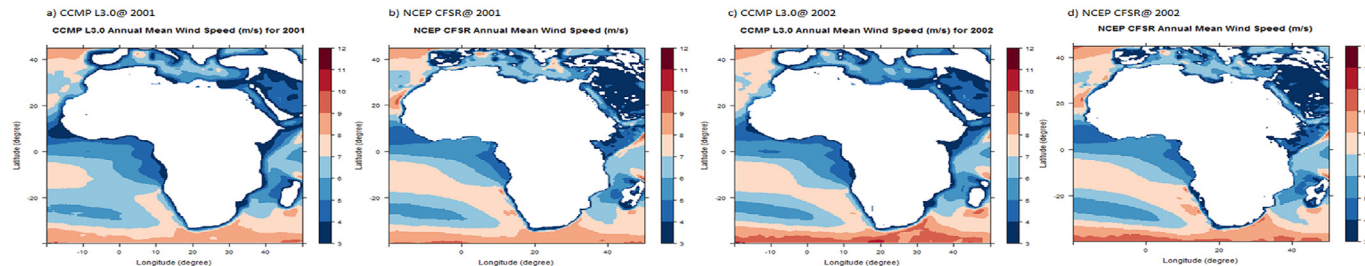


Fig. 7. Annual mean wind speeds at 10 m height derived from CCMP L3.0 and NCEP CFSR for period of 2001–2002.

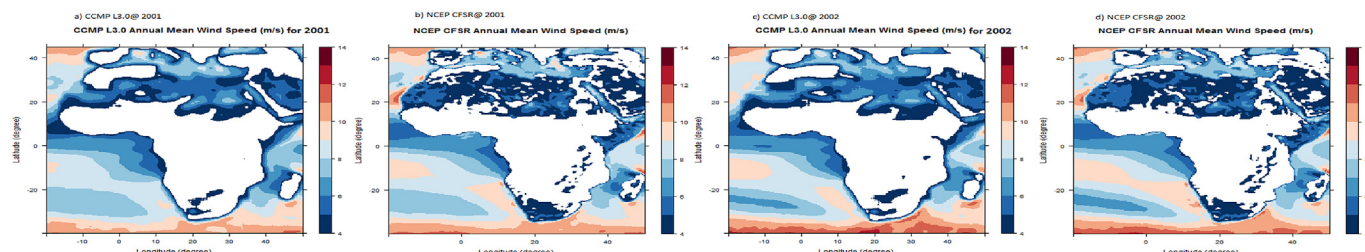


Fig. 8. Annual mean wind speeds at 100 m height derived from CCMP L3.0 and NCEP CFSR for period of 2001–2002.

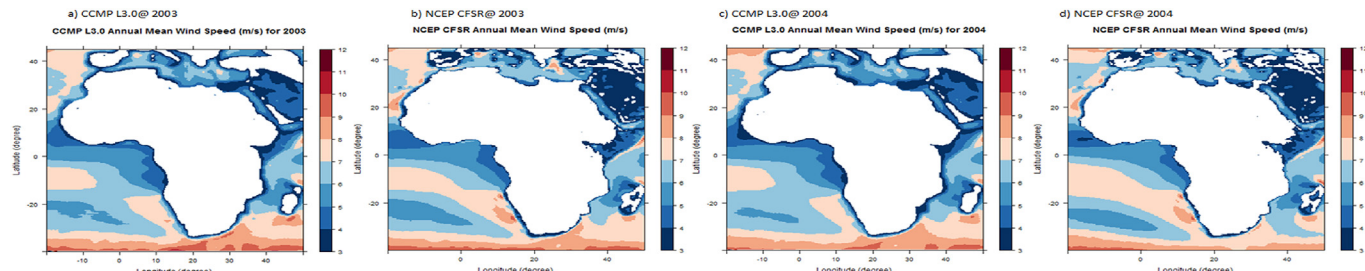


Fig. 9. Annual mean wind speeds at 10 m height derived from CCMP L3.0 and NCEP CFSR for period of 2003–2004.

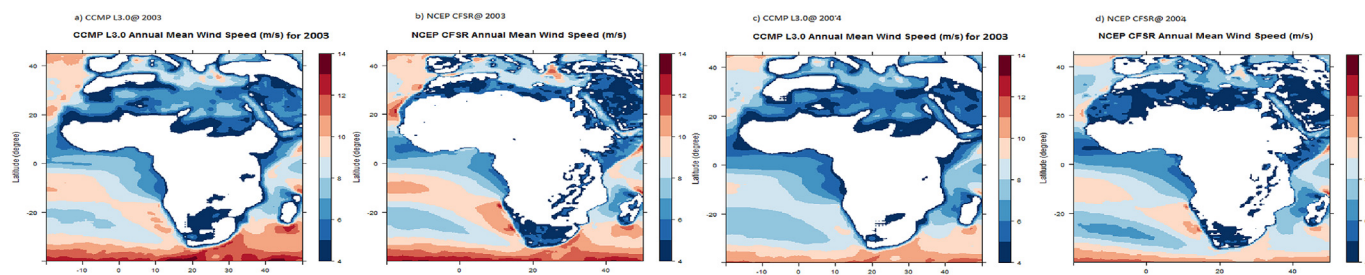


Fig. 10. Annual mean wind speeds at 100 m height derived from CCMP L3.0 and NCEP CFSR for period of 2003–2004.

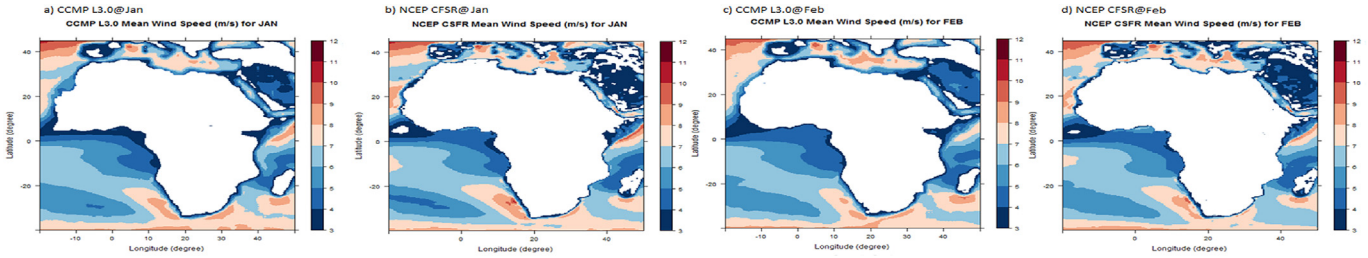


Fig. 11. Inter-month mean wind speeds at 10 m height derived from CCMP L3.0 and NCEP CFSR for Jan 2001–Jan 2010 and Feb 2001–Feb 2010, respectively.

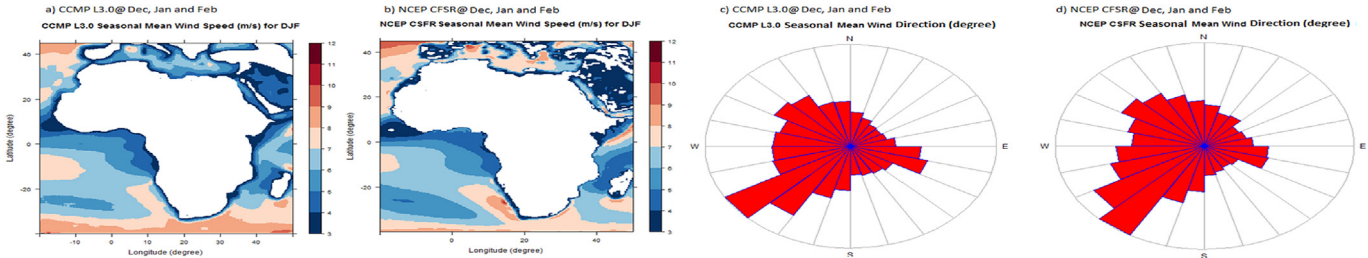


Fig. 12. Seasonal months (DJF) mean wind speeds and sectorwise directions at 10 m height derived from CCMP L3.0 and NCEP CFSR for period of 2001–2010.

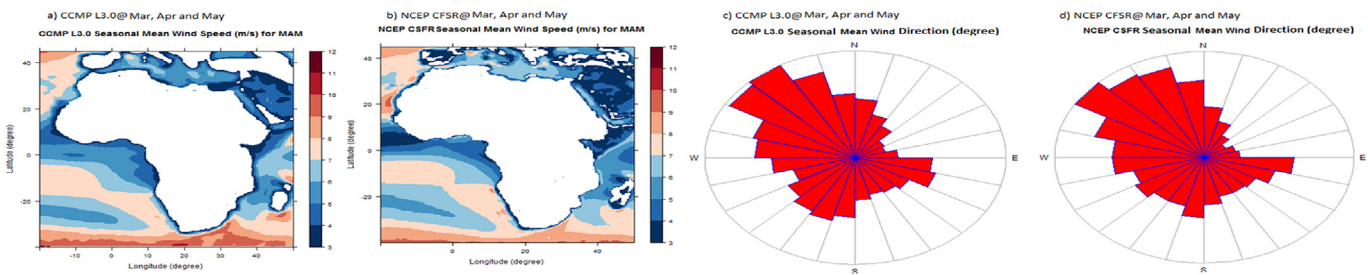


Fig. 13. Seasonal months (MAM) mean wind speeds and sectorwise directions at 10 m height derived from CCMP L3.0 and NCEP CFSR for period of 2001–2010.

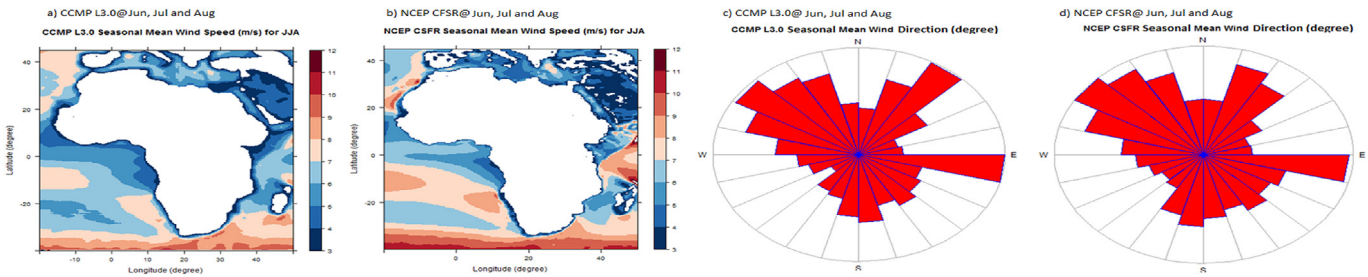


Fig. 14. Seasonal months (JJA) mean wind speeds and sectorwise directions at 10 m height derived from CCMP L3.0 and NCEP CFSR for period of 2001–2010.

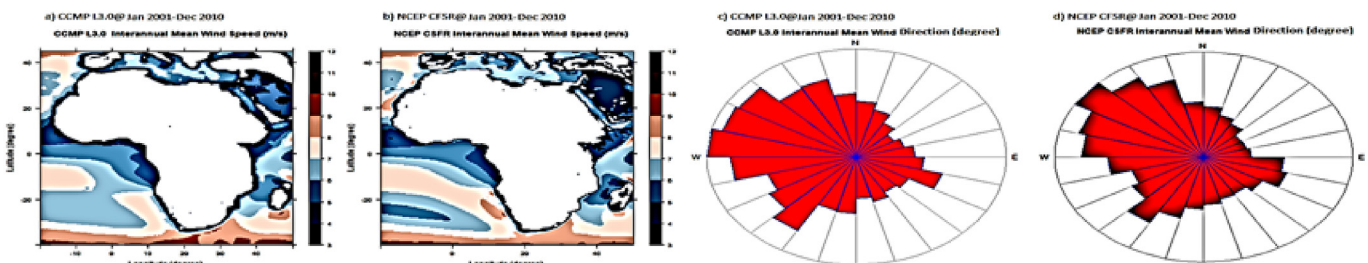


Fig. 15. Seasonal months (SON) mean wind speeds and sectorwise directions at 10 m height derived from CCMP L3.0 and NCEP CFSR for period of 2001–2010.

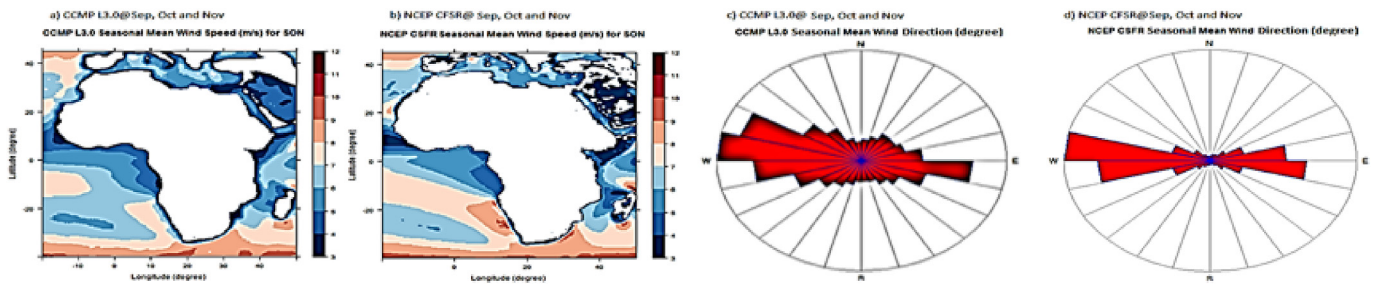


Fig. 16. Inter-annual mean wind speeds and sectorwise directions at 10 m height derived from CCMP L3.0 and NCEP CFSR for period of 2001–2010.

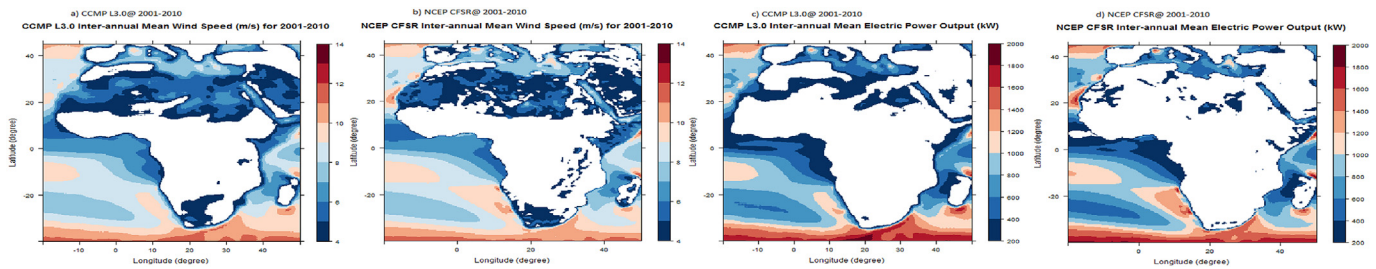


Fig. 17. Inter-annual mean wind speeds and electric power outputs of 2000 kW WTG at 100 m height derived from CCMP L3.0 and NCEP CFSR.

important seasonal months (Mar, JJA and SON) as recorded (Figs. 14 and 15, S7a–b, S10c–d and S11). From Figs (Figs. 2–6 and 12–16), the analyzed SST as well as the sectorwise wind flows across the coasts show that the SW is expected to witness a significant drift (notable slowdown and small increase) of the offshore wind conditions in the nearest future which may span across large portion of the SE coast. From 2001 to 2010, the wind speeds variability across some areas of the SW and E regions shows a significant coastal warming trend along the African region (Figs a–b of 16–17 and S1–S6).

The inter-seasonal trends of the coastal wind anomalies (Fig. 19, S19–S20), annual (Figs. S21–S25) and the inter-annual (Figs. S26–S27) variations of the offshore wind distributions were compared. From comparisons (DJF vs. MAM, Fig. 19a–b), a major change and strong variance of the surface mean winds within ± 2.5 m/s was recorded at the SW-, SE- and N- coasts linked to transition from summer (DJF) to autumn (MAM) weather processes (Figs c–d of 12–13). The seasonal wind distributions in winter (JJA) were also compared to MAM (Fig. 19c and d); a higher variation of the offshore winds (within ≤ 4 m/s) was recorded at few locations farther the W- and E-coast while the S- and SE-coasts had a weak spatial variance of the wind speed (≤ 2 m/s). From the close look at the prevailing offshore wind conditions in DJF to MAM, Fig. 19a and b indicates that the transition from summer to autumn seems to have high spatial variation and impact on wind power harvesting at the S- coast than transition from MAM to JJA (Fig. 19c and d). Moreover, the seasonal bias of the offshore wind distribution derived from the CCMP was compared with NCEP (Fig. 19a vs. 19b and 19c vs. 19d). From the findings, the seasonal patterns of the offshore winds show that the NCEP may be considered for replicating the seasonal wind speeds and not for very short-term wind energy trading. Furthermore, the inter-seasonal (SON with DJF, SON with JJA (Fig. S19); SON with MAM, Fig. S20) mean wind biases (E, m/s) derived from CCMP and NCEP were also compared. At 10 m height, a large portion of the coastal regions of the SW, SE and S had experienced a slight increase of offshore wind speeds (≤ 2 m/s) in Figs. S19a–b. For the comparisons of spring (SON) with JJA (Figs. S19c–d), the smooth transition to spring weather processes

led to stronger spatial variability of the offshore wind (≤ 5.5 m/s). Further to this, from the comparisons of the SON with MAM (Fig. S20), the CCMP and NCEP both indicate a weaker variance with very small increase of the offshore winds (≤ 1.2 m/s) around the SW and SE with exception at very few coastal areas.

The deviations of annual wind speed distributions have been determined (Figs. S21–25) in 1st January to 31st December. From the comparisons, the NCEP tends to average out the wind speed errors over 1-year period. The variance of the NCEP may have been induced by aggregated errors of the time series wind (u- and v-component) during pre- or post-processing over the African coast. Thus, Figs. S21–S25 suggest that the local features/surface stress of NCEP model may have been responsible for large errors in the processed winds on annual basis. On the other hand, the inter-annual mean wind biases derived from NCEP have been compared to CCMP at 10 and 100 m. From Figs. S26–S27, the spatial distribution of the NCEP inter-annual winds was identical to the CCMP (Fig. a–b), with negative mean bias at 10 m and positive wind bias at 100 m. The negative and positive biases denote significant increase or/and change in the offshore wind speed patterns across the coasts from the boundary layer height of 10–100 m. The changes in coastal wind speed pattern were subjects to different weather systems of the Atlantic and Indian Coast of Africa [43].

The estimated mean values of the annual and inter-annual WPDs (W/m^2) across the entire coast and for grids (G1–G4, P1–P3) were summarized (Figs. S12–S13, Col. 7 of Table 1). From the estimated inter-annual mean WPDs at 10 m, G1 recorded much higher wind energy flux at 532 W/m^2 (9.34 m/s); followed by G4 with estimated mean value of 465 W/m^2 (9.06 m/s) while G2 recorded a mean value of 379 W/m^2 (8.23 m/s) while G3 had considerable low mean value of 128 W/m^2 (5.76 m/s). Comparing the magnitude of the offshore WPDs from G1 –G4 (Fig. 1a), result findings indicate that G1 and G4 both had an abundance of offshore wind conditions with slowdown trend from the South Atlantic (S) to W- coast and Indian Ocean (E). Across the entire coastal map, it could be observed that a high energetic flux was dominant at the SE with peak inter-annual mean value of 973 W/m^2 at 100 m (Figs k of S12–13). From the distributions of the annual WPDs derived from

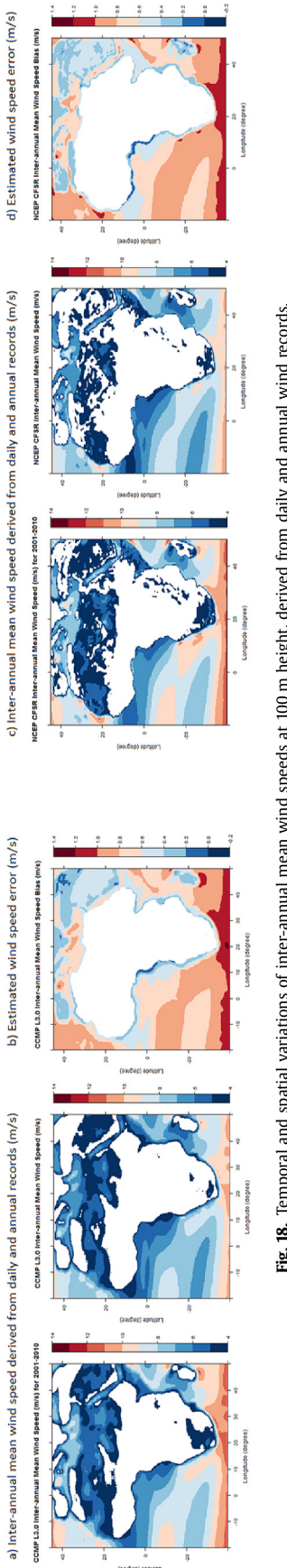


Fig. 18. Temporal and spatial variations of inter-annual mean wind speeds at 100 m height, derived from daily and annual wind records.

CCMP (Fig. S12), the estimated mean WPDs were as follow: 300–882 W/m² in 2001, 300–1167 W/m² in 2002, 300–1580 W/m² in 2003, 300–956 in 2004, 300–1157 in 2005, 300–1004 in 2006, 300–1335 in 2007, 300–1145 in 2008, 300–1120 W/m² in 2009, and 300–1173 W/m² in 2010. Thus, higher wind energy fluxes in 2003 (Fig c) and 2007 (Fig g) at SE coast were dominant. Across the north region, the peak WPDs at 100 were also recorded at: 726 W/m², 904, 894, 686, 617, 740, 635, 700, 633 and 736 W/m² from 2001 to 2010, respectively. From these estimates, it could be observed that the N- coast (44.875°N, -19.875°E) had peak WPD values in 2002 (Fig b) and 2003 (Fig c). With estimated mean WPDs between values of 300 and 1580 W/m², the SE coast falls within wind power class of 3 (fair) to 7 (excellent), capturing the best wind conditions. To quantify the global wind conditions in the N, S, E and W- coasts, the offshore wind resource along the coast of China at 90 m [32] was compared to our results on the African offshore at a 100 m. Abundant wind resource was reported at S- and E-coasts of China with the maximum WPD at 800 W/m² while the maximum WPD value of 1580 W/m² was recorded for S- coast of Africa. This result finding also indicates that the S- coast of Africa possessed higher wind resource as compared to the abundant offshore wind resource reported for coasts of China. In another development, the findings of the offshore resource assessment at a 100 m on the Bohai and Yellow Sea (BYS) of China were compared to study findings of the African coast at 100 m [25]. The inter-annual wind speeds and WPDs range between mean values of 7.0–7.5 m/s and 300–500 W/m² in the BYS zones, respectively, while the offshore mean values for the SE-coast of Africa were estimated at 8.10–13.70 m/s and 300–1580 m/s, respectively. Thus, the SE coast had a huge energy resource as compared to BYS of China at 100 m height.

To characterize the electric power potential and the capacity factor of a typical WTG model, Fig. 17 analyzed the inter-annual electric power outputs of a 2000 kW WTG derived from the simulated CCMP and NCEP winds while Figs. S14–18 represented the annual mean power outputs at 100 m between 2001 and 2010. Considering the promising and potential field (SE) of the African coast, the annual mean of electric power outputs, operating capacity factor (C_p) and offshore winds, v (m/s) (Figs. S14–18), were: 786–1723 kW, 0.451–0.484 and 8.27–11.30 m/s, respectively, in 2001; 786–1903 kW, 0.422–0.484 and 8.24–12.40 m/s in 2002; 936–1982 kW, 0.426–0.485 and 8.24–13.70 m/s in 2003; 786–1629 kW, 0.436–0.478 and 8.26–10.86 m/s in 2004; 786–1903 kW, 0.428–0.485 and 8.27–12.36 m/s in 2005; 756–1825 kW, 0.433–0.485 and 8.17–11.78 m/s in 2006; 786–1958 kW, 0.420–0.484 and 8.30–12.96 m/s in 2007; 672–1903 kW, 0.424–0.484 and 8.10–12.30 m/s in 2008; 786–1894 kW, 0.429–0.484 and 8.28–12.23 m/s in 2009; 756–1894 kW, 0.431–0.485 and 8.20–12.21 m/s in 2010. From the annual mean analysis, it could be observed that the peak energetic (936–1982 kW and C_p of 0.426–0.485) of the model was recorded in 2003, followed by 2005 (786–1903 kW and 0.428–0.485). For the inter-annual electric power outputs, C_p and v (m/s), the mean values at 100 m were estimated: 924–1866 kW, 0.428–0.485 and 8.25–12.00 m/s, respectively (Fig. 17). From the above analysis across this energetic coast (SE), it could be observed that an increase in electric power outputs was predominant from 2001 to 2003 with peak generation at 1982 kW for maximum winds of 13.70 m/s. Similar trends were also observed from 2006 to 2007 with significant increase in the electric power output and magnitude of offshore wind conditions for peak values at 1903 kW and 12.30 m/s, respectively. By comparing the electric power rating of the model to the mean power outputs, result findings show that the offshore wind conditions at 100 m (between 4.00 and 15.00 m/s) could achieve the name-plate power rating of 2000 kW model. To achieve a low operating capacity and higher power outputs for the

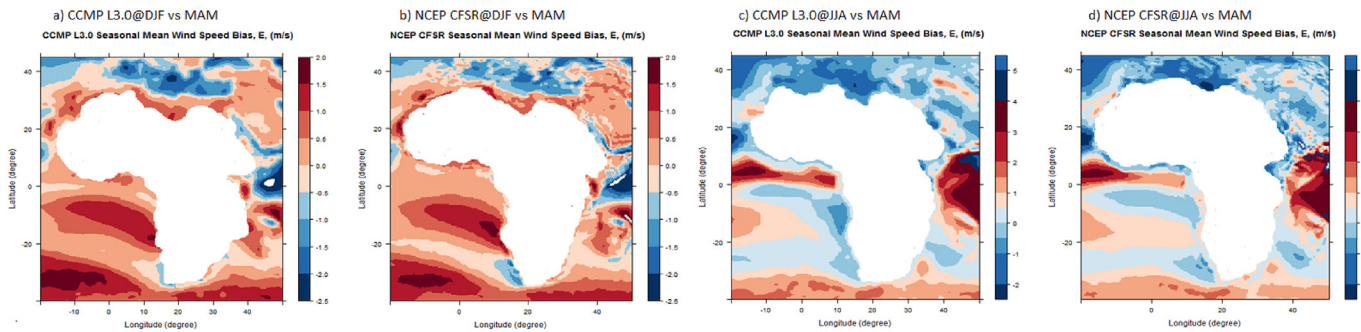


Fig. 19. Inter-seasonal (DJF vs. MAM and JJA vs. MAM) mean wind speed error (E , m/s) at 10 m height derived from CCMP L3.0 and NCEP CFSR for period of 2001–2010.

same **height**, and **cut-in and rated speed**, a higher model (V117-4 MW and V164-8.0 MW) could be utilized, characterized by very strong wind conditions. In addition, the selection of a 2000 kW WTG was not an ideal model for optimization of the coastal wind conditions as the model design with operational conditions ranging between $v_{in} = 3.50$ and $v_{rated} = 13.50$ m/s would produce higher power generation than the selected model ($v_{in} = 4.0$ m/s and $v_{rated} = 15.0$ m/s).

Lastly, the studied findings at 100 m hub were compared to the previous work at 160 m height. The coastal WPDs (W/m^2), estimated C_p and electric power output of 20000 kW model at 100 m were compared to previous studied findings at 3000 kW WTG at 160 m [50]. The inter-annual mean WPDs at the promising coast (SE) were estimated at 580–973 W/m^2 (Figs k of S12–S13) at 100 m and 792–1685 W/m^2 at 160 m. Also, electric power generation of 2000 kW model was simulated at 924–1866 kW (Fig. 17 c-d) and 2410–3000 kW for 3000-kW model (Fig. 6f [50]). For the C_p of the WTG models, the inter-annual mean values were estimated: 0.428–0.485 and 0.320–0.420 at 100 and 160 heights, respectively. From the above analysis, the energetic wind conditions for higher electric power outputs with lower C_p of 3000 kW model were available and accessible at 160 m as compared to the wind energy resource at 100 m. Thus, it's essential in offshore energy optimization to consider the long-term trends of coastal winds at different hubs by considering the seasonal, annual and inter-annual distributions of the offshore wind profiles across the African coast.

4.2.2. Analyzed wind conditions—southwest coast only (Jan–Dec 2002)

To determine if perturbations had resulted in drift/slowdown of the sectorwise wind resource at 10 and 100 m heights, the SW wind conditions within a nested wind field ($\text{lon}_1 = -20^\circ\text{E}$ to $\text{lon}_2 = 0^\circ\text{E}$, $\text{lat}_1 = -40^\circ\text{N}$ to $\text{lat}_2 = 45^\circ\text{N}$) in Columns 2–5 of [Tables 5 and 6](#) were extracted from African coastal zones ($\text{lon}_1 = -20^\circ\text{E}$ to $\text{lon}_2 = 50^\circ\text{E}$, $\text{lat}_1 = -40^\circ\text{N}$ to $\text{lat}_2 = 45^\circ\text{N}$) of [Fig. 1a](#) (rows 2–5 of Cols 2–3 in [Table 1](#)). For the monthly and seasonal satellite observations, these were summarized in [Fig. 20a–p](#). From the figures, the satellite monitoring of the coastal wind conditions indicates the SW and SE coasts to be promising zones for offshore wind power conversion.

The CCMP monthly wind distributions at 10 m at the coastal zones for selected months ([Fig. 22](#)) were compared with wind speed maps at 100 m ASL ([Fig. 23](#)). A significant increase in the monthly wind conditions from mean values of 0–12 m/s at 10 m ([Fig. 22](#)) to 3.0–15 m/s at 100 m ([Fig. 23](#)) was observed. Also, monthly wind speed maps ([Figs. 22 and 23](#)) shows small drift of the monthly wind patterns at SW- and SE-coasts from 10 to 100 m height. From the regional wind circulations in DJF to SON, the seasonal wind flow patterns for the SW strongly agree with the wind conditions at 10 m along the coastal zones ([Fig. 21](#)). That is,

divergence of the offshore wind flows from the S- towards SW-coast with the N- and S-winds converging at the Equator but with higher wind flow magnitude in winter (6.80) followed by summer (5.51), spring (5.47) and autumn (5.31).

For the SW coast only, the sectorwise wind conditions at 100 m ([Fig. 28](#)) for seasonal periods (DJF–SON) revealed that the south-south-easterly (SSE) winds were predominant, followed by the west-north-westerly (WNW), easterly (E) and north–north-easterly (NNE) winds. Also, the sectorwise wind flows at 100 m for the SW coast ([Fig. 28](#)) strongly agree with: ¹the reported finding for coastal regions with predominantly excellent wind conditions at SSE zone based on satellite observations ([Fig. 20m-p](#)), ²the sectorwise wind flows (coasts and land) at 100 m derived from CCMP and NCEP ([Figs a-d of 25 and 27](#)). Furthermore, by comparing the sectorwise wind flows at the SW ([Fig. 28](#)) with the seasonal wind flows ([Figs a-d of 25 and 27](#)), results reveal that local perturbations (weather processes) were responsible for the seasonal drifts of the coastal winds while the seasonal wind variations on land/coastline was subject to combination of the weather processes and topography. It was assumed that if the perturbations arising from local effects doesn't influence the land surface winds across Africa, it was expected that the sectorwise winds in [Figs a-d of 25 and 27](#) to be similar with [Fig. 28](#). For the seasonal winds (SW coast) at 100 m, the estimated wind speed range (m/s), sectorwise winds (N-E-S-W) and the number of wind data-points (N) were summarized (columns 6–8 of [Table 7](#)).

[Fig S36\(a–l\)](#) summarized the monthly wind flows derived from RSS for the SW coast at 100 m. For the months in 2002, the predominant wind conditions were: SSE, WNW, ENE, WSW, N, NNE and ESE winds. In addition, the estimated monthly winds at 10 m hub ([Table 5](#)) were compared with offshore winds at 100 m ([Table 6](#)). Based on the monthly comparisons of [Table 5](#) with 6, the following were observed: ¹the longitude ($\text{lon}_1/\text{lon}_2$) remains the same at 10 and 100 m (Cols 2–3); ²the offshore wind flows within latitudinal boundary ($\text{lat}_1/\text{lat}_2$) had drifted at 10 and 100 m hub (Cols 4–5). That is, the patterns of offshore winds had changed from coordinates ($\text{lat}_1 = -38.625$ and $\text{lat}_2 = 45.0$) of 10 m into new coordinates ($\text{lat}_1 = -40$ and $\text{lat}_2 = 45^\circ\text{N}$) at 100 m; ³the range of mean wind speed (Col 6) and coverage of the sectorwise wind flows (Col 7) had increased (4-ESE to 11-NNW) from 10 m to 100 m; and ⁴the total number of wind data-point (N) from 10 to 100 m (Col 8) had significantly increased by: 500% in Jan, 403 in Feb, 353 in Mar, 334 in Apr, 355 in May, 368 in Jun, 263 in Jul, 446 in Aug, 332 in Sept, 532 in Oct, 389 in Nov and 548% in Dec.

Lastly, the CCMP monthly wind flows (coasts and land) at 10 m were compared with a 100 m for 2002 ([Figs. S33–34](#)). For Jan (Figs a of S33–34), Feb (Figs b) and May (Figs e), similar wind flow trends were observed but with higher intensity at 100 m. The NCEP monthly wind flows (coasts and land) at 10 m ([Fig. S33](#)) were

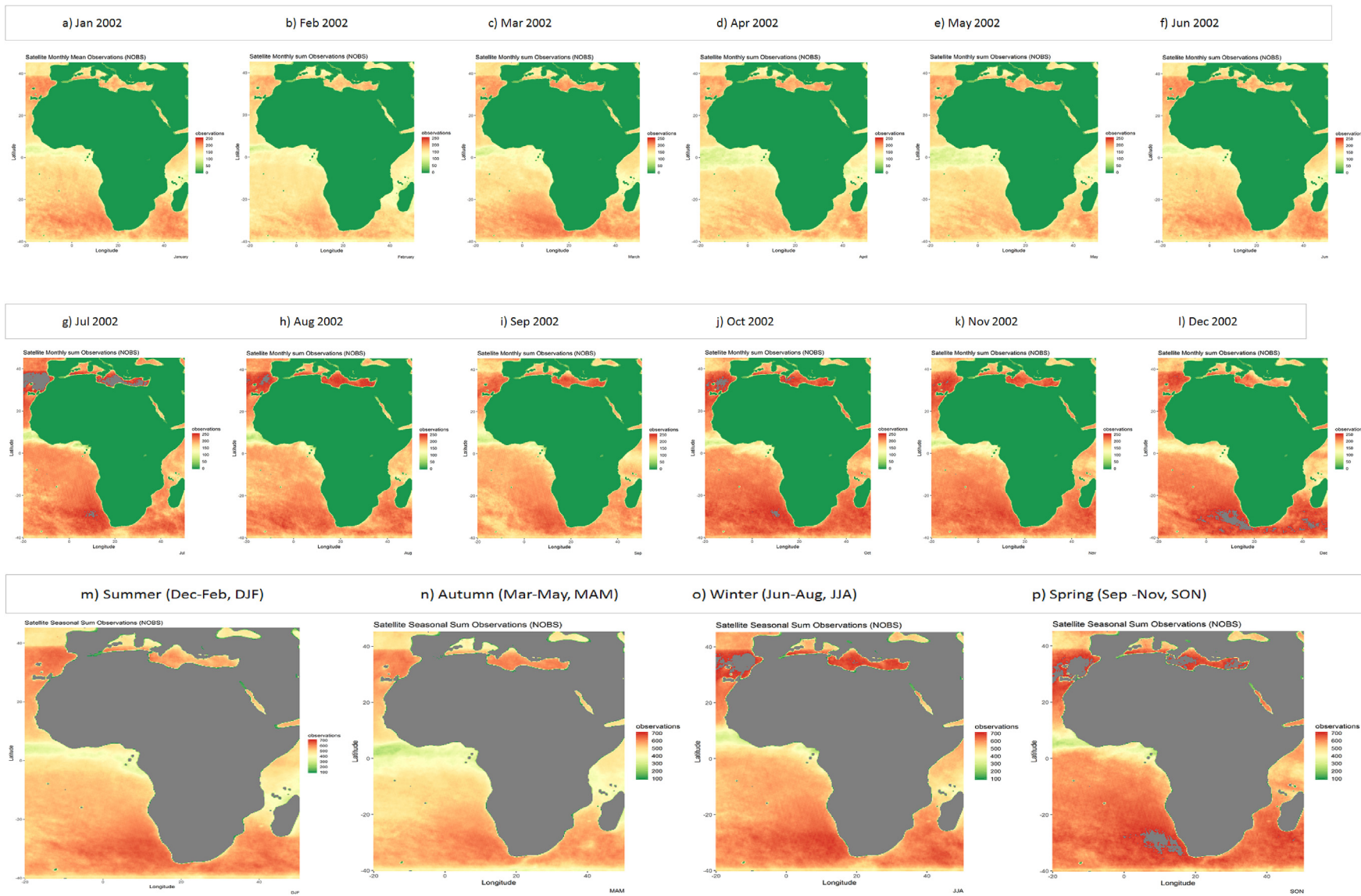


Fig. 20. (a–p): Satellite total number of observations on monthly basis (Jan–Dec) and seasonal (DJF–SON) for the period of 1-year (2002).

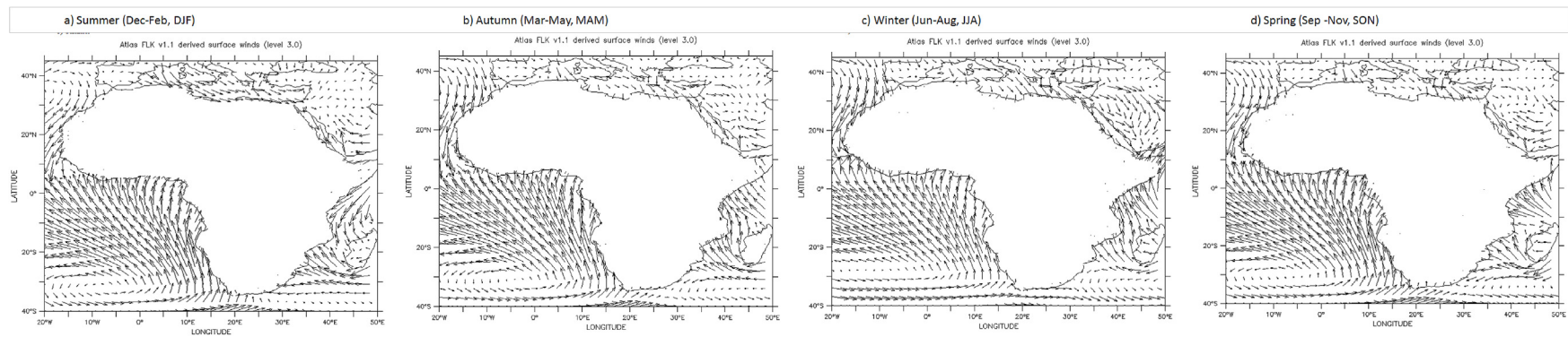


Fig. 21. Satellite seasonal mean wind flow at 10 m height for 2002 along the coastal zones of Africa.

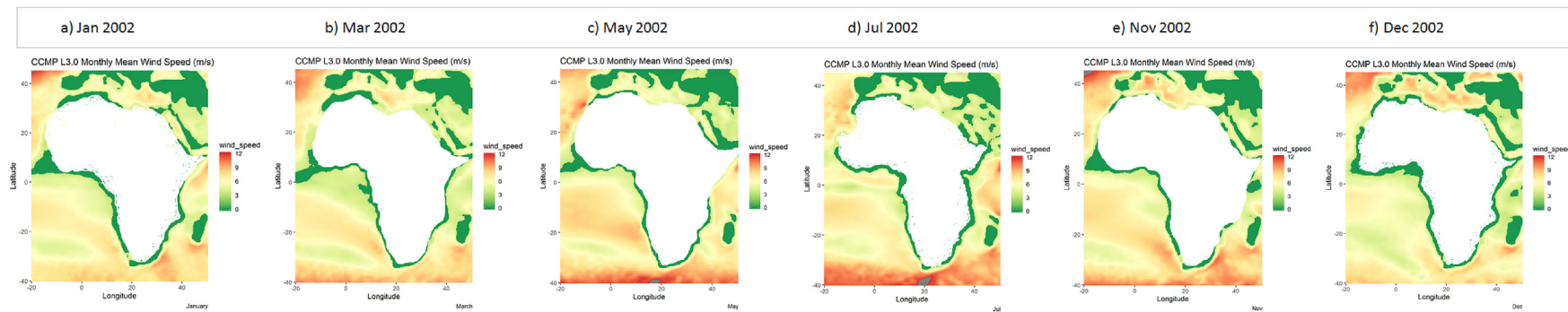


Fig. 22. CCMP L3.0 monthly mean wind speed distribution along the coastal zones of Africa at 10 m height for selected months in 2002.

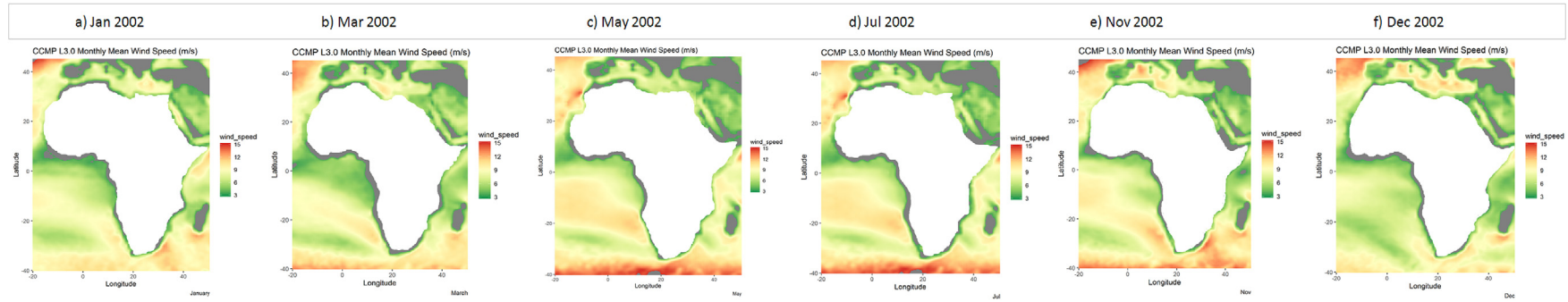
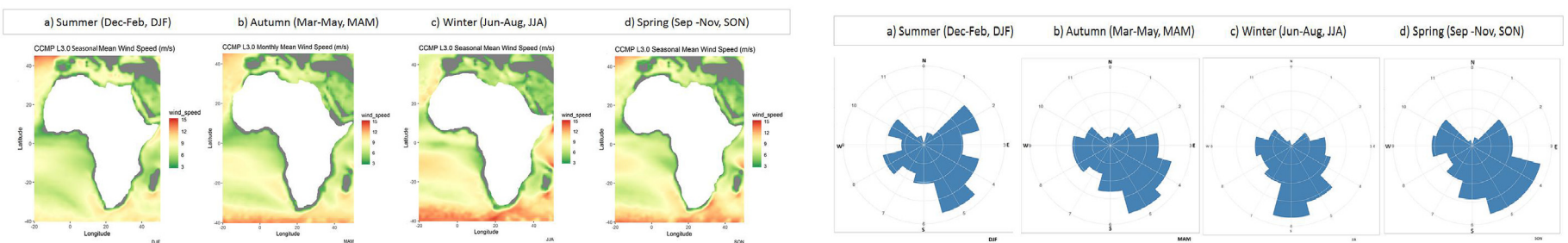
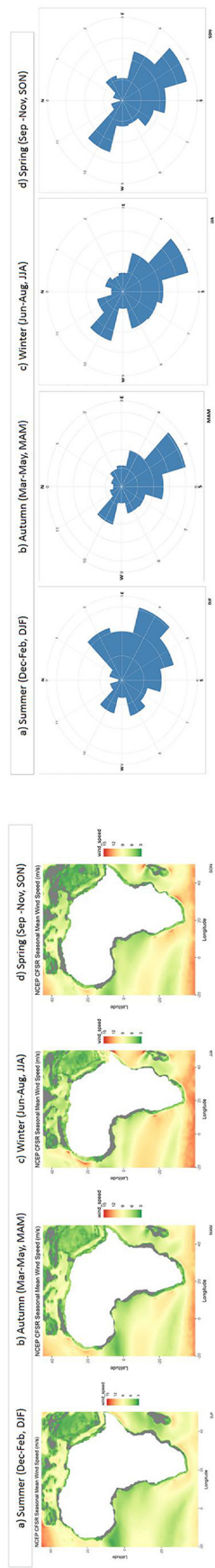


Fig. 23. CCMP L3.0 monthly mean wind speed distribution along the coastal zones of Africa at 100 m height for selected months in 2002.



Figs. 24–25. CCMP L3.0 seasonal mean wind speed distribution along the coastal zones of Africa and sectorwise wind flow (coasts and land surface) at 100 m height for 2002.



Figs. 26–27. NCE CFSR seasonal mean wind speed distribution along the coastal zones of Africa and sectorwise wind flow at 100 m height for 2002.

compared with the CCMP monthly wind flows (coasts and land) at 10 m (Fig. S35). Similar wind flow trends were observed for Jan (Figs a of S33 and 35), Mar–Apr (Figs b–c) and Jun–Dec (Figs f–l). Thus, the comparisons of the sectorwise monthly wind flows at 10 m (Figs. S33 and 35) revealed that the NCEP may be utilized for generalization of the offshore wind conditions (Figs. 24 and 26) where in-situ or station measurements are irretrievable.

5. Summary and conclusions

For the period of 2001–2010, the spatial distributions of the offshore wind conditions driven by the atmospheric circulations had been assessed. Also, it had been shown that the spatial variation of the inter-month and seasonal variations winds was an essential information in the studies of: ¹coastal wind speed anomalies as a function of the sea temperature variations as well as the ²impacts of the variations of offshore wind conditions in electric power generation of the WTG. Furthermore, the comparisons of the NCEP and WRF with CCMP had been used to assess the credibility and limitation of high-resolution models in quantification of the offshore wind conditions across the African coast. From the studied findings at heights of 10 and 100 m, the following conclusions are drawn:

- Within the boundary layer of 100 m height, a large area of the SE experienced a net increase in the near-surface wind conditions with excellent energy resource at the S-coast for wind farm consideration but a slowdown of the boundary layer winds off the SW coast of Africa.
- Farther the SW coast of Africa towards the Equator, convergence of the offshore winds, upward (positive) trend of the SST anomalies with slowdown of the offshore wind conditions while a negative SST with stronger offshore winds over the central South Atlantic was dominant; thus, contributing to a drift of the offshore wind circulations within the boundary layer height of 100 m (that is, negative wind bias at a 10 m and a positive bias at 100 m).
- From 2001 to 2010, offshore areas off the southwest coast were seen to be mostly susceptible to the regional climate changes/ high coastal surface temperature. Thus, the coast of SE is expected to witness a strong drift of the inter-monthly wind flows in the nearest future as a result of changes in the monthly wind flow patterns along the entire coast.
- Although, studied findings show that weather system processes of Atlantics, and East Coast do play significant role in the offshore wind circulations across the entire African coast, however, the coastal energy resource conversion for WTG operations is viable at the considered heights but with higher WTG models for optimization.
- The quantification of the offshore wind conditions show that the offshore energy resource was enhanced in S and SE coasts of Africa with general slowdown off the west coast.
- The concentration and dominant wind energy resource at the offshore could be best explained by the directional flows (SE, SW and NW). Thus, the quantification of the long-term variability of the wind conditions on a regional-scale is essential in power grid planning and expansion.
- The offshore wind flow patterns had drifted from referenced coordinates ($\text{lat1} = -38.625$ and $\text{lat2} = 45.0$) of 10 m into new coordinates ($\text{lat1} = -40$ and $\text{lat2} = 45^{\circ}\text{N}$) at 100 m. Thus, higher wind conditions are available as function of height within the boundary layer of 200 m.
- Studied findings revealed that the NCEP may be utilized for generalization of the offshore wind conditions at the African Coasts where in-situ winds are irretrievable

a) Summer Dec-Feb (DJF) b) Autumn Mar-May (MAM) c) Winter Jun-Aug (JJA) d) Spring Sep-Nov (SON)

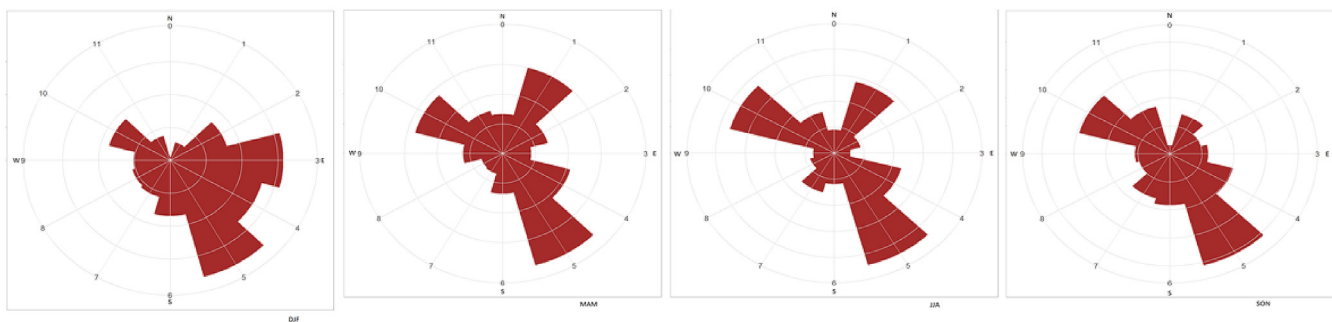


Fig. 28. Satellite seasonal mean wind flow (southwest coast only) for the offshore at 100 m height for 2002.

Table 3

Offshore bi-annual mean wind speed biases (m/s) across the entire coast between 2001 and 2010.

10 m	2001–2002	2002–2003	2003–2004	2004–2005	2005–2006	2006–2007	2007–2008	2008–2009	2009–2010
v_{min} (m/s)	-1.36	-1.10	-1.70	-0.46	-1.28	-0.97	-1.05	-0.83	-2.22
v_{max} (m/s)	1.58	1.24	0.24	1.68	1.14	1.64	0.85	0.81	2.92
100 m	2001–2002	2002–2003	2003–2004	2004–2005	2005–2006	2006–2007	2007–2008	2008–2009	2009–2010
v_{min} (m/s)	-1.64	-0.51	-2.35	-0.74	-1.57	-1.28	-1.33	-1.05	-2.74
v_{max} (m/s)	1.92	2.76	0.31	1.27	1.48	1.86	1.09	1.01	3.63

Table 4

Estimated annual mean wind speeds (m/s) at reference G1-G4 (see Fig. 1a).

Grid points	2001	2002	2003	2004	2005	2006	2007	2008	2009	2010	2001–2010
G1	8.92	10.18	9.60	8.44	9.40	9.80	10.00	9.78	9.49	9.54	9.52
G2	8.72	9.38	8.54	7.74	8.38	8.74	8.14	8.82	8.58	8.60	8.56
G3	6.42	5.78	5.78	5.47	6.05	5.90	5.82	5.85	6.07	6.27	5.94
G4	8.88	9.02	9.00	8.11	9.60	9.18	9.12	9.65	8.94	9.10	9.06

Table 5

Estimated satellite monthly mean wind statistics (southwest coast only) at reference 10 m height for 2002.

Months	lon1(nx ₁) (°E)	lon2(nx ₂) (°E)	lat1(ny ₁) (°N)	lat2(ny ₂) (°N)	Mean wind speed bins (m/s)	Sectorwise winds (N-E-S-W)	Wind speed datapoints (N)
Jan	-20.00	00.00	-38.625	44.375	3.50–8.30	0-N – 3-E	5018
Feb	-20.00	00.00	-36.625	41.125	3.50–8.80	0-N – 2-ENE	6261
Mar	-20.00	00.00	-28.875	41.125	3.50–10.40	0-N – 3-E	7176
Apr	-20.00	00.00	1.125	45.000	3.50–9.10	0-N – 3-E	7454
May	-20.00	00.00	-32.375	39.625	3.50–9.10	0-N – 3-E	7004
Jun	-20.00	00.00	-31.375	36.875	3.50–8.50	0-N – 3-E	6806
Jul	-20.00	00.00	-26.875	44.375	3.50–9.50	0-N – 4-ESE	9427
Aug	-20.00	00.00	-29.625	45.000	3.50–9.40	0-N – 3-E	5415
Sep	-20.00	00.00	-33.875	45.000	3.50–8.70	0-N – 4-ESE	7172
Oct	-20.00	00.00	-28.375	37.125	3.50–7.40	0-N – 4-ESE	4469
Nov	-20.00	00.00	-33.125	34.125	3.50–8.50	0-N – 3-E	6377
Dec	-20.00	00.00	-31.625	32.875	3.50–7.20	0-N – 2-ENE	4544

Finally, for accurate turbine site layout and power grid expansion, the availability of coastal winds at different grids across the African coasts was mainly dependent on the spatial distributions of the coastal wind conditions, operating capacity factor of the selected turbine model for different wind conditions, among

others.

Declaration of competing interest

The Author has no conflict of interest in this work.

Table 6

Estimated satellite monthly mean wind statistics (southwest coast only) at observed 100 m height for 2002.

Months	lon1(nx ₁) (°E)	lon2(nx ₂) (°E)	lat1 (ny ₁) (°N)	lat(ny ₂) (°N)	Mean wind speed bins (m/s)	Sectorwise winds (N-E-S-W)	Wind speed datapoints (N)
Jan	-20.00	0.00	-40.00	45.00	3.50–15.80	0-N – 11-NNW	25099
Feb	-20.00	0.00	-40.00	45.00	3.50–14.00	0-N – 11-NNW	25221
Mar	-20.00	0.00	-40.00	45.00	3.50–13.40	0-N – 11-NNW	25329
Apr	-20.00	0.00	-40.00	45.00	3.50–13.30	0-N – 11-NNW	24887
May	-20.00	0.00	-40.00	45.00	3.50–14.70	0-N – 11-NNW	24844
Jun	-20.00	0.00	-40.00	45.00	3.50–14.30	0-N – 11-NNW	25070
Jul	-20.00	0.00	-40.00	45.00	3.50–14.30	0-N – 11-NNW	24768
Aug	-20.00	0.00	-40.00	45.00	3.50–13.70	0-N – 11-NNW	24150
Sep	-20.00	0.00	-40.00	45.00	3.50–12.70	0-N – 11-NNW	23803
Oct	-20.00	0.00	-40.00	45.00	3.50–14.70	0-N – 11-NNW	23755
Nov	-20.00	0.00	-40.00	45.00	3.50–16.50	0-N – 11-NNW	24777
Dec	-20.00	0.00	-40.00	45.00	3.50–13.70	0-N – 11-NNW	24906

Table 7

Estimated satellite seasonal mean wind statistics (southwest coast only) at 100 m height for 2002 (see Fig. 28).

Months	lon1(nx ₁) (°E)	lon2(nx ₂) (°E)	lat1 (ny ₁) (°N)	lat(ny ₂) (°N)	Mean wind speed bins (m/s)	Sectorwise winds (N-E-S-W)	Wind speed datapoints (N)
DJF	-20.00	0.00	-40.00	45.00	3.50–12.68	0-N – 11-NNW	27076
MAM	-20.00	0.00	-40.00	45.00	3.50–12.60	0-N – 11-NNW	26949
JJA	-20.00	0.00	-40.00	45.00	3.50–12.90	0-N – 11-NNW	26407
SON	-20.00	0.00	-40.00	45.00	3.50–13.80	0-N – 11-NNW	26526

Acknowledgment

CCMP version-2.0 analyses [52] were produced by Remote Sensing Systems and sponsored by NASA Earth Science funding. Satellite ocean wind dataset was freely available at www.remss.com. The local topography and WRF datasets utilized for the three grid points at coast of South Africa were sourced from the WASA project and acknowledged. The NCEP Climate Forecast System Reanalysis (CFSR) data was sourced from <https://rda.ucar.edu/>. Technical supports from Ojelade S., Famuyiwa G. Adebawale E.A are appreciated.

Appendix A. Supplementary data

Supplementary data to this article can be found online at <https://doi.org/10.1016/j.energy.2019.116232>.

References

- [1] d'Arlon Rue. Europe adds 4.5 GW of wind energy in first half of 2018. at, <https://windeurope.org/newsroom/press-releases/europe-adds-4-5-gw-of-wind-energy-in-first-half-of-2018/>. [Accessed 1 October 2018].
- [2] Salvador S, Costoya X, Sanz-Larruga FJ, Gimeno L. Development of offshore wind power: contrasting optimal wind sites with legal restrictions in Galicia, Spain. Energies 2018;11(4):731. <https://dx.doi.org/10.3390/en11040731>.
- [3] Colmenar-Santos A, Perera-Perez J, Borge-Diez D, dePalacio-Rodriguez C. Offshore wind energy: a review of the current status, challenges and future development in Spain. Renew Sustain Energy Rev 2016;64:1–18. <https://dx.doi.org/10.1016/j.rser.2016.05.087>.
- [4] Lled LI, Torralba V, Soret A, Ramon J, Doblas-Reyes FJ. Seasonal forecasts of wind power generation. Renew Energy 2019;143:91–100. <https://doi.org/10.1016/j.renene.2019.04.135>.
- [5] Jung C, Taubert D, Schindler D. The temporal variability of global wind energy – long-term trends and inter-annual variability. Energy Convers Manag 2019;188:462–72. <https://dx.doi.org/10.1016/j.enconman.2019.03.072>.
- [6] Jakub J, Marcin W, Bartosz K, Paweł D. Temporal and spatial complementarity of wind and solar resources in Lower Silesia (Poland). In: International Conference on Advances in energy systems and Environmental Engineering (ASEE17), Wrocław, Poland, E3S Web of Conferences, vol. 22; 2017. id.00074, November 2017, <https://dx.doi.org/10.1051/e3sconf/20172200074>.
- [7] Bierstedt Svenja E, Hünicke Birgit, Zorita Eduardo. Variability of wind direction statistics of mean and extreme wind events over the Baltic Sea region. Tellus A Dyn Meteorol Oceanogr 2015;67(1):1–15. <https://doi.org/10.3402/tellusa.v67.29073>. 29073.
- [8] Banta RM, Pichugina YL, Brewer WA, James EP, Olson JB, Benjamin SG, Carley JR, Bianco L, Djalalova IV, Wilczak JM, Hardesty RM, Cline J, Marquis MC. Evaluating and improving NWP forecast models for the future:
- [9] Floors R, Batchvarova E, Gryning S-E, Hahmann AN, Pena A, Mikkelsen T. Atmospheric boundary layer wind profile at a flat coastal site “wind speed lidar measurements and mesoscale modeling results. Adv Sci Res 2011;6: 155–9. <https://doi.org/10.5194/asr-6-155-2011>.
- [10] Satyanarayana GCh, Supriya RHL, Rao DVB. Wind energy assessment over the Andhra Pradesh and Telangana regions. Meteorol Appl 2019;26(1):14–29.
- [11] Jaagus J, Kull A. Changes in surface wind directions in Estonia during 1966–2008 and their relationships with large-scale atmospheric circulation. Est J Earth Sci 2011;60:220–31.
- [12] Wachsmuth J, Blohm A, Gassling-Reisemann S, Eickemeier T, Ruth M, Gasper R, et al. How will renewable power generation be affected by climate change? The case of a metropolitan region in Northwest Germany. Energy 2013;58:192–201.
- [13] Johansson B. Security aspects of future renewable energy systems: a short overview. Energy 2013;61(1):598–605.
- [14] Khan KS, Muhammad T. Wind resource assessment using SODAR and meteorological mast- A case study of Pakistan. Renew Sustain Energy Rev 2018;81: 2443–9. <https://doi.org/10.1016/j.rser.2017.06.050>.
- [15] Charabi Y, Al Hinai A, Al-Yahyai S, et al. Offshore wind potential and wind atlas over the Oman Maritime Zone, Energy. Ecol Environ 2019;4(1):1–14. <https://doi.org/10.1007/s40974-019-00108-7>.
- [16] Liu Z, Dong Z, Zhang Z, Cui X, Xiao N. Spatial and temporal variation of the near-surface wind regimes in the Taklimakan Desert, Northwest China: Theoretical and applied Climatology. 2019. p. 1–15. <https://doi.org/10.1007/s00704-019-02824-w>.
- [17] Weisse R, Bisling P, Gaslikova L, Geyer B, Groll N, et al. Climate services for marine applications in Europe. Earth Perspective 2015;2(3):1–14.
- [18] Nair Sandhya K, Anurose TJ, Subrahmanyam D Bala, et al. Characterization of the vertical structure of coastal atmospheric boundary layer over thumba during different seasons. Advances in Meteorology 2011;2011:1–9. Article ID 390826, <https://doi.org/10.1155/2011/390826>.
- [19] Natalie Perlin N, de Szoeke S, Chelton DB, O'Neill LW, et al. Modeling the atmospheric boundary layer wind response to mesoscale sea surface temperature perturbations. Mon Weather Rev 2013;142(11):4284–307. <https://doi.org/10.1175/MWR-D-13-0032.1>.
- [20] Zha J, Zhao D, Wu J, Zhang P. Numerical simulation of the effects of land use and cover change on the near-surface wind speed over Eastern China. Clim Dyn 2019:1–21. <https://doi.org/10.1007/s00382-019-04737-w>.
- [21] Ki-Yong O, Ji-Young K, JUN-Shin L, Wahn R. Wind resource assessment around Korean Peninsula for feasibility study on 100 MW class offshore wind farm. Renew Energy 2012;42C:217–26. <https://dx.doi.org/10.1016/j.renene.2011.08.012>.
- [22] Indasi VS, Lynch MJ, McGann B, Sutton J, Yu F, Jeanneret F. Use of mast and remote sensing data for wind resource assessment in Kenya. International Journal of Latest Research in Engineering and Technology 2017;3(3):106–15.
- [23] Draxl C, Clifton A, Hodge BS, McCaa J. The wind integration national dataset (WIND) toolkit. Appl Energy 2015;151:355–66. <https://dx.doi.org/10.1016/j.apenergy.2015.03.121>.
- [24] Onea F, Rusu L. Evaluation of some state-of-the-art wind technologies in the near shore of the black sea. Energies 2018;11(2452):1–16. <https://dx.doi.org/10.3390/en11092452>.

- [25] Li DL, Geyer B, Bisling P. A model-based climatology analysis of wind power resources at 100 m height over the Bohai Sea and the Yellow Sea. *Appl Energy* 2016;179:575–98. <https://dx.doi.org/10.1016/j.apenergy.2016.07.010>.
- [26] Santos F, Gomez-Gesteira M, deCastro M, Anel JA, Carvalho D, Costoya X, Dias JM. On the accuracy of CORDEX RCMs to project future winds over the Iberian Peninsula and surrounding ocean. *Appl Energy* 2018;228:289–300. <https://dx.doi.org/10.1016/j.apenergy.2018.06.086>.
- [27] Carvalho D, Rocha A, Gomez-Gesteira M, Santos CS. Offshore wind energy resource simulation forced by different reanalyses: comparison with observed data in the Iberian Peninsula. *Appl Energy* 2014;134:57–64. 2014, <https://dx.doi.org/10.1016/j.apenergy.2014.08.018>.
- [28] Banta RM, Pichugina YL, Brewer WA, James EP, Olson JB, Benjamin SG, et al. Evaluating and improving NWP forecast models for the future: how the needs of offshore wind energy can point the way. *Bull Am Meteorol Soc* 2018;99(6): 1155–76. <https://dx.doi.org/10.1175/BAMS-D-16-0310.1>.
- [29] Hasager CB, Astrup P, Zhu R, Chang R, Badger M, Hahmann AN. Quarter-century offshore winds from SSM/I and WRF in the north Sea and south China sea. *Remote Sens* 2016;8(9):769. <https://dx.doi.org/10.3390/rs8090769>.
- [30] Koizumi A, Kubota M, Kutsuwada K. "Impact of usage of multiple-satellite sensors on accuracy of sea surface wind Data,"^À 2018 Progress in Electromagnetics Research Symposium. Toyama: PIERS-Toyama); 2018. p. 1366–71. <https://doi.org/10.23919/PIERS.2018.8598002>.
- [31] Balsamo G, Agusti-Panareda A, Albergel C, Zeng X, et al. Satellite and *in situ* observations for advancing global Earth surface modeling: a review. *Remote Sens* 2018;10(12):2038. <https://doi.org/10.3390/rs10122038>.
- [32] Liu Y, Chen D, Li S, Chan PW. Discerning the spatial variations in offshore wind resources along the coast of China via dynamic downscaling. *Energy* 2018;160:582–96.
- [33] Chang R, Zhu R, Badger M, Hasager CB, Xing X, Jiang Y. Offshore wind resources assessment from multiple satellite data and WRF modeling over south China sea. *Remote Sens* 2015;7:467–87. <https://dx.doi.org/10.3390/rs70100467>.
- [34] Zheng M, Li XM, Sha JJ. Comparison of sea surface wind field measured by HY-2 scatterometer and WindSat in global oceans. *J Oceanol Limnol* 2018;1–9. <https://dx.doi.org/10.1007/s00343-019-7347-2>.
- [35] Xu Q, Li Y, Li X, Zhang Z, Cao Y, Cheng Y. Impact of ships and ocean fronts on coastal sea surface wind measurements from the advanced scatterometer. *IEEE J Sel Top Appl Earth Obs Remote Sens* 2018;99:1–8. <https://dx.doi.org/10.1109/JSTARS.2018.2817568>.
- [36] Gadad S, Deka PC. Offshore wind power resource assessment using Oceansat-2 scatterometer data at a regional scale. *Appl Energy* 2016;176:157–70. <https://dx.doi.org/10.1016/j.apenergy.2016.05.046>.
- [37] Jang J-K, Yu B-M, Ryu K-W, Lee J-S. Offshore wind resource assessment around Korean Peninsula by using QuikSCAT satellite data. *J Korean Soc Aeronaut Space Sci* 2009;37(11):1121–30. <https://dx.doi.org/10.5139/JKSAS.2009.37.11.1121>.
- [38] James EP, Benjamin SG, Marquis M. Offshore wind speed estimates from a high-resolution rapidly updating numerical weather prediction model forecast dataset. *Wind Energy* 2017;21(4). <https://dx.doi.org/10.1002/we.2161>.
- [39] Cunden TSM, Dhunny AZ, Lollchund MR, Rughooputh SDDV. Sensitivity analysis of WRF model for wind modelling over a complex topography under extreme weather conditions. In: 5th International Symposium on Environment-Friendly Energies and applications (EFEA). Rome (Italy): IEEE Explore; 2018. p. 1–6. <https://doi.org/10.1109/EFEA.2018.8617050>.
- [40] Gholamreza A, Somayeh M, Said M. Offshore wind resource assessment of Persian Gulf using uncertainty analysis and GIS. *Renew Energy* 2017;113: 915–29. <https://doi.org/10.1016/j.renene.2017.06.070>.
- [41] Kumar AS, Prajapati J, Kumar R. Offshore wind energy potential assessment of India based on the synergistic use of QuikSCAT, OSCAT and ASCAT scatterometers data. In: Proceedings of the Fourth International Conference in ocean Engineering (ICOE2018), vol. 23; 2019. p. 823–34. Singapore, https://doi.org/10.1007/978-981-13-3134-3_61.
- [42] Larsen XG, Mann J. Extreme winds from the NCEP/NCAR reanalysis data. *Wind Energy* 2009;12:556–73.
- [43] Bhat S, Jain P, Deo MC. Application of regional climate models for coastal design parameters along India. *J Coast Res* 2018. <https://dx.doi.org/10.2112/JCOASTRES-D-17-00145.1>.
- [44] Luzzatto-Fegiz P, Caulfield CP. Entrainment model for fully-developed wind farms: effects of atmospheric stability and an ideal limit for wind farm performance. *Phys Rev Fluids* 2018;3(9):093802. <https://doi.org/10.1103/PhysRevFluids.3.093802>.
- [45] Yonglong L, Jingjing Y, Li Q, Chao S, et al. Impacts of land-based human activities on coastal and offshore marine ecosystems. *Acta Ecol Sin* 2016;36(5): 1183–91. <https://doi.org/10.5846/stxb201511182334>.
- [46] Gomez-Gesteira M, deCastro M, Alvarez I, Gomez-Gesteira JL. Coastal sea surface temperature warming trend along the continental part of the Atlantic Arc (1985–2005). *J Geophys Res* 2008;113:1–9. C04010, <https://doi.org/10.1029/2007JC004315>.
- [47] Yu L, Zhong S, Bian X, Heilman WE. Temporal and spatial variability of wind resources in the United States as derived from the Climate Forecast System Reanalysis. *J Clim* 2015;28(3):1166–83. <https://doi.org/10.1175/JCLI-D-14-00322.1>.
- [48] Kulkarni S, Deo MC, Ghosh S. Performance of the CORDEX regional climate models in simulating offshore wind and wind potential. *Theor Appl Climatol* 2018;1–16. <https://doi.org/10.1007/s00704-018-2401-0>.
- [49] Greene JS, Chatelain M, Morrissey M, Stadler S. Projected future wind speed and wind power density trends over the western US high plains. *Atmos Clim Sci* 2012;2:32–40. <https://dx.doi.org/10.4236/acs.2012.2100545>.
- [50] Olaofe ZO. Review of energy systems deployment and development of offshore wind energy resource map at the coastal regions of Africa. *Energy* 2018;161:1096–114.
- [51] Bagiorgas HS, Mihalakakou G, Rehman LS, AL-Hadhrami LM. Offshore wind speed and wind power characteristics for ten locations in Aegean and Ionian Seas. *J. Earth Syst. Sci.* 2012;121(4):975–87. 2012.
- [52] a Atlas R, Hoffman RN, Ardizzone J, Leidner SM, Jusem JC, Smith DK, Gombos D. A cross-calibrated, multiplatform ocean surface wind velocity product for meteorological and oceanographic applications. *Bull Am Meteorol Soc* 2011;92:157–74. <https://doi.org/10.1175/2010BAMS2946.1.b> NASA/GSFC/NOAA. Cross-calibrated Multi-Platform ocean surface wind Vector L3.0 First-look analyses. 2009. PO.DAAC, CA, USA, Version 1. <https://dx.doi.org/10.5067/CCF30-01XXX>. [Accessed 5 November 2016]. at.